

Superfluid flow in disordered superconductors with Dynes pair-breaking scattering: depairing current, kinetic inductance, and superheating field

Takayuki Kubo*

*High Energy Accelerator Research Organization (KEK), Tsukuba, Ibaraki 305-0801, Japan and
The Graduate University for Advanced Studies (Sokendai), Hayama, Kanagawa 240-0193, Japan*

We investigate the effects of Dynes pair-breaking scattering rate Γ on the superfluid flow in a narrow thin-film superconductor and a semi-infinite superconductor by self-consistently solving the coupled Maxwell and Usadel equations for the BCS theory in the diffusive limit for all temperature T , all Γ , and all superfluid momentum. We obtain the depairing current density $j_d(\Gamma, T)$ and the current-dependent nonlinear kinetic inductance $L_k(j_s, \Gamma, T)$ in a narrow thin-film and the superheating field $H_{sh}(\Gamma, T)$ and the current distribution in a semi-infinite superconductor, taking the nonlinear Meissner effect into account. The analytical expressions for $j_d(\Gamma, T)|_{T=0}$, $L_k(j_s, \Gamma, T)|_{T=0}$, and $H_{sh}(\Gamma, T)|_{T=0}$ are also derived. The theory suggests j_d and H_{sh} can be ameliorated by reducing Γ , and L_k can be tuned by a combination of the bias current and Γ . Tunneling spectroscopy can test the theory and also give insight into how to engineer Γ via materials processing. Implications of the theory would be useful to improve performances of various superconducting quantum devices.

I. INTRODUCTION

The physics of the superfluid flow in s -wave superconductors is closely tied with the operating principles and performances of various superconducting quantum devices such as superconducting nanowire single-photon detectors (SNSPDs) [1, 2], resonators for microwave kinetic inductance detectors (MKIDs) [3, 4] and quantum computers [5–7], and superconducting radio-frequency (SRF) resonant cavities for particle accelerators [8–11]. The supercurrent density j_s is proportional to the superfluid momentum $\hbar q$ and the superfluid density n_s . When $|q|$ is such a small value that n_s is not significantly suppressed, j_s linearly increases with $|q|$. However, as $|q|$ increases, the reduction of n_s becomes significant, and j_s ceases to increase [12–14]. The maximum value of j_s is called the depairing current density j_d and determines the stability limit of the superfluid flow, above which finite electrical resistance necessarily appears. In SNSPDs, a superconducting nanowire is biased with a dc current close to j_d . An incident photon absorbed by the strip heats electrons and reduces the critical current below the bias current, resulting in measurable finite electrical resistance. The reset time after a detection event is often limited by the kinetic inductance [15]. In MKIDs, the kinetic inductance plays an essential role in its operating mechanism. Incoming photons with a frequency higher than the superconducting gap break Cooper pairs and lead to an increase of the kinetic inductivity $L_k \propto 1/n_s$. A resultant shift of resonant frequency $\delta f \propto -\delta L_k$ can be detected. Besides, the bias current also reduces n_s and increase L_k and can be utilized to tune a resonator frequency [16] and to observe the nonlinear Meissner Effect [17]. In SRF resonant cavities, charged particles are accelerated by the electric component of the microwave, which is proportional to the rf magnetic field at the sur-

face. Vortex-free cavities [18–20] exhibit huge quality factor $Q \sim 10^{10}$ – 10^{12} at $T < 2$ K [21–23] even under the strong rf magnetic field [24–27] such that the nonlinear Meissner effect manifest itself. Here the achievable rf field is limited by the induced screening current at the surface, which cannot exceed j_d . The surface magnetic field that induces j_d is coincident with the superheating field H_{sh} , which is the stability limit of the Meissner state. H_{sh} is thought to define the upper limit of the accelerating field [9–11] and is one of the main interests in fundamental SRF studies [28, 29].

Microscopic calculations of physical quantities relevant to these devices would provide us with a deeper understanding of experimental results and clues to improving device performances. Those for disordered materials are especially important because these devices are often made from high-resistance films or impurity-doped bulk materials [30–34]. Some 60 years ago, Maki calculated j_d at the temperature $T \rightarrow 0$ [13, 14]. Kupriyanov and Lukichev obtained j_d for an arbitrary T [35]. By using the Maki's results, L_k for the current-carrying state was calculated afterwards [36]. Then those for all T and all j_s up to j_d were investigated [37]. Calculations of H_{sh} also have a long history, starting from those for a clean-limit superconductor [38, 39]. Effects of homogeneous [40] and inhomogeneous [41] impurities on H_{sh} were recently investigated. Yet, theories including realistic materials features which can limit device performances have been studied lesser extent. Such theories would be useful to pin down causes of performance limitations, e. g., critical current below the ideal j_d in nanowires and quenches below the ideal H_{sh} in SRF cavities, etc.

One of the common features among various superconducting materials is the broadening of the density of states (DOS), which has been observed in a numerous number of tunneling experiments [42] (see e.g., Refs. [31, 43, 44] for SRF materials). Such a broadened DOS has been described by the Dynes formula [45, 46], which is given by $N(\epsilon)/N_0 = \text{Re}[(\epsilon + i\Gamma)/\sqrt{(\epsilon + i\Gamma)^2 - \Delta^2}]$ (see

* kubotaka@post.kek.jp

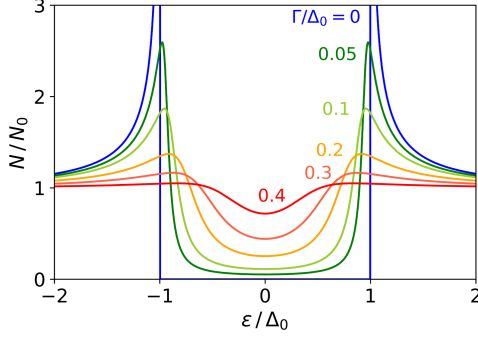


FIG. 1. Quasiparticle DOS calculated for $T/T_{c0} = 0.2$ and $\Gamma/\Delta_0 = 0, 0.05, 0.1, 0.2, 0.3, 0.4$. Here Δ_0 is the BCS pair potential at $T = 0$ and T_{c0} is the BCS critical temperature for $\Gamma = 0$.

Fig. 1). Here Γ is the Dynes pair-breaking scattering rate, resulting in a finite density of subgap states in the vicinity of the Fermi level Γ/Δ and a constant quasiparticle lifetime \hbar/Γ . A microscopic derivation of the Dynes formula has been investigated [47–49]. Besides, independent of microscopic models of Dynes formula, it is possible to formulate the quasiclassical theory of the BCS model which incorporates Γ [50–52]. Interestingly, it has been shown that the pair-breaking Γ parameter and other pair breakers (e.g., current [54–56], magnetic impurities [57, 58] and proximity-coupled normal layer [59, 60]) can reduce the rf dissipation in the weak- and the strong-rf regimes via a modification of the quasiparticle spectrum [50–53].

In this work, we focus on effects of Γ on the superfluid flow in disordered superconductors. We consider the geometries shown in Fig. 2: a thin and narrow superconducting film (relevant to, e.g., SNSPD, MKID) and a semi-infinite superconductor (relevant to, e.g., SRF cavities made from bulk materials or thick film). We evaluate the depairing current density $j_d(\Gamma, T)$, the current-dependent nonlinear kinetic inductance $L_k(j_s, \Gamma, T)$, and the superheating field $H_{sh}(\Gamma, T)$ for all T , all Γ , and all current. The results of this work would provide with clues to finding out causes of performance limitations and those used to improve performances of superconducting quantum devices.

The paper is organized as follows. In Section II, we briefly review the Eilenberger-Usadel formalism [61–64] of the BCS theory and express physical quantities with the Matsubara Green’s functions. In Sec. III, we solve the Usadel equation for all T , all Γ , and all q . Some useful formulas of Δ , n_s , λ , and j_s at $T = 0$ and $\simeq T_c$ are also obtained. In Sec. IV, we consider a thin and narrow superconducting film [Fig. 2 (a)]. We evaluate the depairing current density $j_d(\Gamma, T)$ and the current-dependent nonlinear kinetic inductance $L_k(j_s, \Gamma, T)$. In addition to numerical results, we present the analytical formulas for $j_d(\Gamma, T)$ and $L_k(j_s, \Gamma, T)$ at $T = 0$ and $\simeq T_c$. In Sec. V, we consider a semi-infinite superconductor

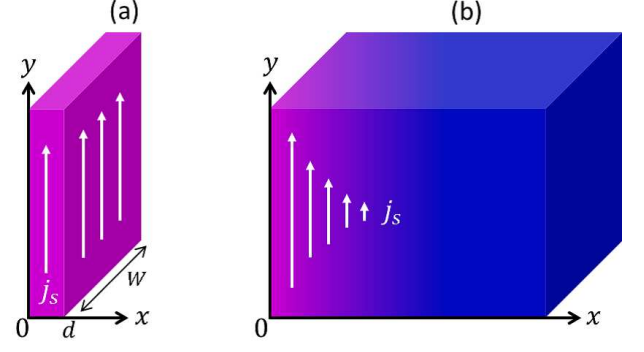


FIG. 2. (a) Thin and narrow superconducting film carrying a uniform current j_s . We assume a thickness $d \ll \lambda$ and a width $W \ll \lambda^2/d$. (b) Semi-infinite superconductor carrying the Meissner current $j_s(x)$. We assume λ is much larger than the coherence length.

[Fig. 2 (b)]. We calculate the current distribution taking the nonlinear Meissner effect into account and evaluate the superheating field $H_{sh}(\Gamma, T)$. Analytical formula for $T \rightarrow 0$ and $T \simeq T_c$ are also derived. In Sec. VI, we discuss the implications of our results.

II. THEORY

We apply the well-established Eilenberger-Usadel formalism [61–64] of the BCS theory in the diffusive limit to the geometries shown in Fig. 2. The normal and anomalous quasiclassical Matsubara Green’s functions $G_{\omega_n} = \cos \theta$ and $F_{\omega_n} = \sin \theta$ obey the Usadel equation:

$$\frac{\hbar D}{2} \theta'' = s \sin \theta \cos \theta + (\hbar \omega_n + \Gamma) \sin \theta - \Delta \cos \theta. \quad (1)$$

Here D is the electron diffusivity, the prime denotes differentiation with respect to x , $s = (q/q_\xi)^2 \Delta_0$ is the superfluid flow parameter, $\Delta_0 = \Delta(s, \Gamma, T)|_{s=\Gamma=T=0}$ is the BCS pair potential at $T = 0$, $\hbar q = 2mv_s$ is the superfluid momentum, v_s is the superfluid velocity, m is the electron mass, $q_\xi = \sqrt{2\Delta_0/\hbar D}$ is the inverse of the coherence length, and $\hbar \omega_n = 2\pi k_B T(n + 1/2)$ is the Matsubara frequency. In Figs. 2 (a) and 2 (b), the current distributes uniformly and varies slowly over the coherence length, respectively. In either cases, the θ'' term is negligible and Eq. (1) reduces to

$$\left(\Delta - \frac{s}{\sqrt{1 + \cot^2 \theta}} \right) \cot \theta = \hbar \omega_n + \Gamma. \quad (2)$$

Note that, in Fig. 2 (b), θ and Δ depend on x via $s = s(x)$. The pair potential $\Delta(s, \Gamma, T)$ satisfies the self-consistency equation

$$\ln \frac{T_{c0}}{T} = 2\pi k_B T \sum_{\omega_n > 0} \left(\frac{1}{\hbar \omega_n} - \frac{\sin \theta}{\Delta} \right), \quad (3)$$

where $k_B T_{c0} = \Delta_0 \exp(\gamma_E)/\pi \simeq \Delta_0/1.76$ is the BCS critical temperature, and $\gamma_E = 0.577$ is the Euler constant. The thermodynamic critical field H_c is given by [49, 52]

$$H_c(\Gamma, T) = \sqrt{-\frac{2}{\mu_0} \Omega(0, \Gamma, T)}, \quad (4)$$

$$\Omega(0, \Gamma, T) = -2\pi T N_0 \Delta \times \sum_{\omega_n > 0} \left[\frac{2(\hbar\omega_n + \Gamma)}{\Delta} (\cos \theta - 1) + \sin \theta \right], \quad (5)$$

where θ and Δ in Eq. (5) are evaluated for $s = 0$. The superfluid density n_s , penetration depth λ and supercurrent density j_s are given by

$$\frac{n_s(s, \Gamma, T)}{n_{s0}} = \frac{\lambda_0^2}{\lambda^2(s, \Gamma, T)} = \frac{4k_B T}{\Delta_0} \sum_{\omega_n > 0} \sin^2 \theta, \quad (6)$$

$$\frac{j_s(s, \Gamma, T)}{j_{s0}} = \sqrt{\frac{\pi s}{\Delta_0}} \frac{n_s(s, \Gamma, T)}{n_{s0}}. \quad (7)$$

Here $n_{s0} = n_s(0, 0, 0) = 2\pi m N_0 D \Delta_0 / \hbar$ is the BCS superfluid density at $T = 0$, $\lambda_0 = \lambda(0, 0, 0) = \sqrt{\hbar / \pi \mu_0 \Delta_0 \sigma_n}$ is the BCS penetration depth at $T = 0$, $j_{s0} = H_{c0} / \lambda_0 = \sqrt{\pi} |e| N_0 D \Delta_0 q_\xi$, and $H_{c0} = H_c(0, 0) = \sqrt{N_0 / \mu_0 \Delta_0}$ is the BCS thermodynamic critical field at $T = 0$.

In the geometry shown in Fig. 2 (b), n_s , λ , and j_s depend on x through $s(x) = [q(x)/q_\xi]^2 \Delta_0$. Here $j_s(x)$, $H(x)$, and $q(x)$ obey the Maxwell equation, $j_s = -\partial_x H$ and $\mu_0 H = (\hbar/2|e|) \partial_x q$, namely,

$$\frac{\partial^2 q}{\partial x^2} = \frac{q}{\lambda^2(s, \Gamma, T)}, \quad (8)$$

$$\frac{H}{H_{c0}} = \sqrt{\pi} \frac{\partial(q/q_\xi)}{\partial(x/\lambda_0)}. \quad (9)$$

By using the magnetic field at the surface H_0 , the boundary conditions can be written as

$$H(0) = H_0, \quad \lim_{x \rightarrow \infty} q(x) \rightarrow 0. \quad (10)$$

Self-consistent calculations of Eqs. (2), (3), and (6)-(10) yield the distributions of $\theta(x)$, $\Delta(x)$, $\lambda(x)$, $j_s(x)$, $q(x)$, and $H(x)$ for a given set of H_0 and T .

In the Ginzburg-Landau (GL) regime, $T \simeq T_c$, we can expand the Matsubara Green's functions in powers of $\delta = \Delta / 2\pi k_B T \ll 1$ [52]:

$$\sin \theta = a\delta - \frac{1}{2} \left(a^3 - \frac{s}{2\pi k_B T} a^4 \right) \delta^3, \quad (11)$$

$$\cos \theta = 1 - \frac{a^2}{2} \delta^2 - \frac{1}{8} \left(\frac{2s}{\pi k_B T} a^5 - 3a^4 \right) \delta^4. \quad (12)$$

Here $a = (n + 1/2 + s/2\pi k_B T + \Gamma/2\pi k_B T)^{-1}$. Substituting Eqs. (11) and (12) into Eq. (3), we obtain the GL equation [52],

$$1 - \frac{T}{T_c} = \frac{\pi s}{4k_B T_c} + \frac{7\zeta(3)}{8\pi^2 k_B^2 T_c^2} \Delta^2, \quad (13)$$

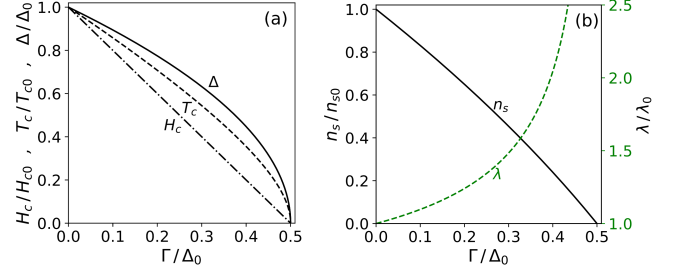


FIG. 3. (a) $\Delta(0, \Gamma, T)|_{T \rightarrow 0}$, $T_c(\Gamma)$, $H_c(\Gamma, T)|_{T \rightarrow 0}$, (b) $n_s(0, \Gamma, T)|_{T \rightarrow 0}$, and $\lambda(0, \Gamma, T)|_{T \rightarrow 0}$ as functions of Γ .

for Δ , s , $\Gamma \ll 2\pi k_B T$ and $T \simeq T_c$. Note here T_c depends on Γ .

In the following, we use Δ_0 as a unit of energy and use dimensionless quantities $\tilde{s} = s/\Delta_0$, $\tilde{\omega}_n = \hbar\omega_n/\Delta_0$, $\tilde{\Gamma} = \Gamma/\Delta_0$, $\tilde{\Delta} = \Delta/\Delta_0$, $\tilde{T} = k_B T/\Delta_0$, etc. For brevity, we omit all these tildes.

III. SOLUTIONS

A. Zero-current state ($s = 0$)

First, consider the zero-current state ($s = 0$) at the low-temperature limit ($T = 0$). The pair potential Δ can be calculated from Eqs. (2) and (3). The solution of Eq. (2) is given by $\cot \theta = (\hbar\omega_n + \Gamma)/\Delta$. Substituting θ into Eq. (3), we find (see Appendix A)

$$\Delta(0, \Gamma, 0) = \exp \left[-\sinh^{-1} \frac{\Gamma}{\Delta(0, \Gamma, 0)} \right], \quad (14)$$

which reduces to $\Delta \simeq 1 - \Gamma$ for $\Gamma \ll 1$. The equation for T_c is obtained by solving Eqs. (2) and (3) for $(\theta, \Delta) \ll 1$ and $T \simeq T_c$. Then, we have [50, 52],

$$\ln \frac{T_c}{T_{c0}} = \psi \left(\frac{1}{2} \right) - \psi \left(\frac{1}{2} + \frac{\Gamma}{2\pi T_c} \right), \quad (15)$$

which reduces to $T_c \simeq T_{c0} - \pi\Gamma/4$ for $\Gamma \ll 1$. The thermodynamic critical field H_c can be calculated from Eqs. (4) and (5). At $T = 0$, we find (see Appendix A)

$$\frac{H_c(\Gamma, 0)}{H_{c0}} = \Delta \sqrt{1 + \frac{2\Gamma^2}{\Delta^2}} - \frac{2\Gamma}{\Delta} \sqrt{1 + \frac{\Gamma^2}{\Delta^2}}, \quad (16)$$

which reduces to $H_c/H_{c0} \simeq 1 - 2\Gamma$ for $\Gamma \ll 1$. The superfluid density n_s and the penetration depth λ can be calculated from Eq. (6). At $T = 0$, we have [50, 52]:

$$\begin{aligned} \frac{n_s(0, \Gamma, 0)}{n_{s0}} &= \frac{\lambda_0^2}{\lambda^2(0, \Gamma, 0)} \\ &= \Delta(0, \Gamma, 0) \left[1 - \frac{2}{\pi} \tan^{-1} \frac{\Gamma}{\Delta(0, \Gamma, 0)} \right], \end{aligned} \quad (17)$$

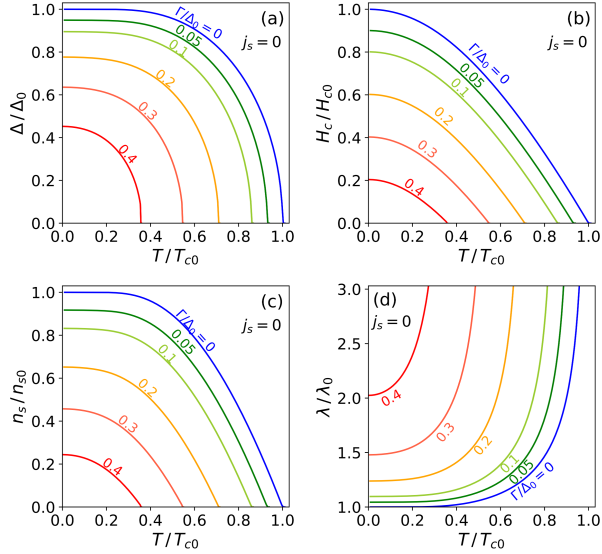


FIG. 4. (a) $\Delta(0, \Gamma, T)$, (b) $H_c(\Gamma, T)$, (c) $n_s(0, \Gamma, T)$, and (d) $\lambda(0, \Gamma, T)$ as functions of T calculated for different Γ .

which reduces to $n_s/n_{s0} \simeq 1 - (1 + 2/\pi)\Gamma$ for $\Gamma \ll 1$. Shown in Fig. 3 are $\Delta(0, \Gamma, T)|_{T=0}$, $T_c(\Gamma)$, $H_c(\Gamma, T)|_{T=0}$, and $n_s(0, \Gamma, T)|_{T=0}$ as functions of Γ , which monotonically decrease as Γ increases and vanish at $\Gamma = 1/2$.

For $T \simeq T_c$, the GL regime, we can calculate Δ from Eq. (13). Then, we have [52]

$$\Delta(0, \Gamma, T) = \sqrt{\frac{8\pi^2 T_c^2}{7\zeta(3)} \left(1 - \frac{T}{T_c}\right)}, \quad (18)$$

$$H_c(\Gamma, T) = \sqrt{\frac{8\pi^2 T_c^2 N_0}{7\zeta(3)\mu_0} \left(1 - \frac{T}{T_c}\right)}, \quad (19)$$

$$\frac{n_s(0, \Gamma, T)}{n_{s0}} = \frac{\lambda_0^2}{\lambda^2(0, \Gamma, T)} = \frac{4\pi^2 T_c}{7\zeta(3)} \left(1 - \frac{T}{T_c}\right), \quad (20)$$

for $T \simeq T_c(\Gamma)$. Here Eqs. (4)-(6) are used. Eqs. (18)-(20) are coincident with the usual GL results for the zero-current state. The only difference is that T_c depends on Γ through Eq. (15).

For $0 < T < T_c$, we numerically solve Eqs. (2)-(6). Shown in Fig. 4 are $\Delta(0, \Gamma, T)$, $H_c(\Gamma, T)$, $n_s(0, \Gamma, T)$, and $\lambda(0, \Gamma, T)$ as functions of T . Then, Δ , H_c , and $n_s \propto \lambda^{-2}$ are monotonically decreasing functions of T and Γ [49, 50, 52].

B. Current-carrying state ($s > 0$)

Now consider the current-carrying state ($s > 0$). In addition to the Dynes pair-breaking scattering rate Γ , the superfluid momentum q give rise to pair-breaking effects, suppressing Δ and n_s and resulting in nonlinearity of j_s respect with q .

For $T = 0$, the self-consistency equation results in (see Appendix B)

$$\Delta(s, \Gamma, 0) = \exp \left[-\sinh^{-1} u_0 - \frac{s}{2\Delta(s, \Gamma, 0)} \left(\frac{\pi}{2} - \tan^{-1} u_0 - \frac{u_0}{1 + u_0^2} \right) \right], \quad (21)$$

where $u_0(s, \Gamma)$ is defined by $[\Delta(s, \Gamma, 0) - s/\sqrt{1 + u_0^2}]u_0 = \Gamma$. The superfluid density $n_s(s, \Gamma, 0)$ can be calculated from Eq. (6). Hence (see Appendix B)

$$\frac{n_s(s, \Gamma, 0)}{n_{s0}} = \frac{\lambda_0^2}{\lambda^2(s, \Gamma, 0)} = \Delta(s, \Gamma, 0) \left[1 - \frac{2}{\pi} \tan^{-1} u_0 \right] - \frac{4s}{3\pi} \left\{ 1 - \frac{u_0(3 + 2u_0^2)}{2(1 + u_0^2)^{3/2}} \right\}. \quad (22)$$

Note that Eqs. (21) and (22) reproduce Eqs. (14) and (17) at the zero-current limit ($s \rightarrow 0$). The supercurrent density j_s is calculated from Eq. (7):

$$j_s(s, \Gamma, 0) = \sqrt{\pi s} \frac{n_s(s, \Gamma, 0)}{n_{s0}} \frac{H_{c0}}{\lambda_0}. \quad (23)$$

The set of Eqs. (21)-(23) are the general formulas for $\Delta(s, \Gamma, T)|_{T=0}$, $n_s(s, \Gamma, T)|_{T=0}$, $\lambda(s, \Gamma, T)|_{T=0}$, and $j_s(s, \Gamma, T)|_{T=0}$ valid for all current and all Γ . When $\Gamma = 0$, the well-known Maki's formulas [13, 14, 37] are reproduced.

For $\Gamma \ll 1$ such that $u_0 = \Gamma/(\Delta - s) \ll 1$, Eqs. (21)-(23) reduce to the approximate formulas:

$$\Delta(s, \Gamma, 0) = \exp \left[-\frac{\pi s}{4\Delta(s, \Gamma, 0)} - \frac{\Gamma}{\Delta(s, \Gamma, 0)} \right], \quad (24)$$

$$\frac{n_s(s, \Gamma, 0)}{n_{s0}} = \frac{\lambda_0^2}{\lambda^2(s, \Gamma, 0)} = \Delta(s, \Gamma, 0) - \frac{4s}{3\pi} - \frac{2\Gamma}{\pi}, \quad (25)$$

$$j_s(s, \Gamma, 0) = \sqrt{\pi s} \left[\Delta(s, \Gamma, 0) - \frac{4s}{3\pi} - \frac{2\Gamma}{\pi} \right] \frac{H_{c0}}{\lambda_0}. \quad (26)$$

For $(s, \Gamma) \ll 1$, Eqs. (24)-(26) reduce to even simpler formulas:

$$\Delta(s, \Gamma, 0) = 1 - \frac{\pi s}{4} - \Gamma, \quad (27)$$

$$\begin{aligned} \frac{n_s(s, \Gamma, 0)}{n_{s0}} &= \frac{\lambda_0^2}{\lambda^2(s, \Gamma, 0)} \\ &= 1 - \left(\frac{\pi}{4} + \frac{4}{3\pi} \right) s - \left(1 + \frac{2}{\pi} \right) \Gamma, \end{aligned} \quad (28)$$

$$j_s(s, \Gamma, 0) = \sqrt{\pi s} \left[1 - \left(\frac{\pi}{4} + \frac{4}{3\pi} \right) s - \left(1 + \frac{2}{\pi} \right) \Gamma \right] \frac{H_{c0}}{\lambda_0}. \quad (29)$$

Eqs. (24)-(26) are valid under an arbitrary current density as long as Γ satisfies $\Gamma/(\Delta - s) \ll 1$. Eqs. (27)-(29) are useful when we consider the small-current regime.

Shown in Fig. 5 are Δ , n_s , j_s at $T = 0$ as functions of the superfluid momentum $|q/q_\xi| = \sqrt{s}$ calculated from the exact formulas given by Eqs. (21)-(23). While Δ and

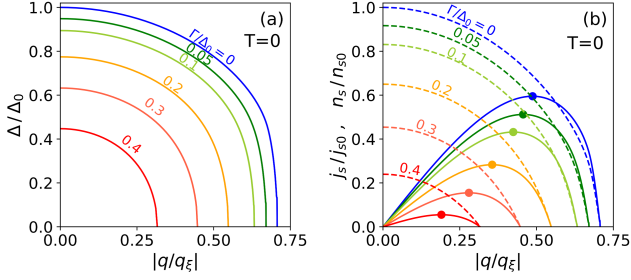


FIG. 5. $\Delta(s, \Gamma, T)|_{T=0}$, $n_s(s, \Gamma, T)|_{T=0}$, and $j_s(s, \Gamma, T)|_{T=0}$ calculated from the formulas given by Eqs. (21)-(23). (a) Δ , (b) j_s (solid curves) and n_s (dashed curves) as functions of $|q/q_\xi| (= \sqrt{s})$ for different Γ . Each colored blob represents the maximum current density, namely, the depairing current density.

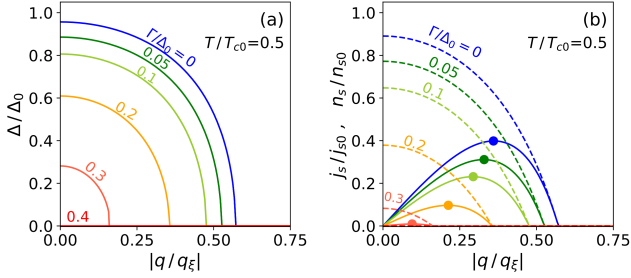


FIG. 6. $\Delta(s, \Gamma, T)$, $n_s(s, \Gamma, T)$, and $j_s(s, \Gamma, T)$ at a finite temperature obtained by numerically solving Eqs. (2)-(7). (a) Δ , (b) j_s (solid curves) and n_s (dashed curves). Note that a superconductor with $\Gamma = 0.4$ (red) has $T_c = 0.36T_{c0} < T$, being normal for all q .

$n_s(\propto \lambda^{-2})$ are monotonically decreasing functions, j_s exhibits non-monotonic behaviors. At smaller $|q|$ regions, j_s is proportional to $|q|$. As $|q|$ increases, j_s becomes dominated by a rapid reduction of n_s and ceases to increase. At a threshold value q_d or $s_d = (q_d/q_\xi)^2$, j_s reaches the maximum value (colored blob), which is the depairing current density j_d .

For $T \simeq T_c$, the GL regime, Δ in the current-carrying state is calculated from Eq. (13). Then, we obtain [52]

$$\Delta(s, \Gamma, T) = \sqrt{\frac{8\pi^2 T_c^2}{7\zeta(3)} \left(1 - \frac{T}{T_c}\right) \left(1 - \frac{s}{s_m}\right)}, \quad (30)$$

$$\frac{n_s(s, \Gamma, T)}{n_{s0}} = \frac{\lambda_0^2}{\lambda^2(s, \Gamma, T)} = \frac{\Delta^2(s, \Gamma, T)}{2T_c}, \quad (31)$$

$$j_s(s, \Gamma, T) = \sqrt{\frac{\pi}{2(T_c - T)}} \sqrt{s} \left(1 - \frac{s}{s_m}\right) \frac{H_c(\Gamma, T)}{\lambda(0, \Gamma, T)} \quad (32)$$

for $T \simeq T_c(\Gamma)$. Here $s_m(\Gamma, T) = (4T_c/\pi)(1 - T/T_c)$.

For $0 < T < T_c$, we need to numerically solve Eqs. (2)-(7) for a finite s . Shown in Figs. 6 (a) and 6 (b) are $\Delta(s, \Gamma, T)$, $n_s(s, \Gamma, T)$, and $j_s(s, \Gamma, T)$ as functions of $|q/q_\xi| = \sqrt{s}$ at $T/T_{c0} = 0.5$ for different Γ . The simi-

lar calculations for other T are straightforward (see also Ref. [52]). The q dependences of Δ , n_s , and j_s resemble those for $T = 0$ (see Fig. 5). As T increases, all these values monotonically decrease, and the depairing current densities (colored blobs) also shift to lower values.

IV. THIN AND NARROW FILM

In this section, we consider the geometry shown in Fig. 2 (a): a narrow thin-film. We calculate the depairing current density and the kinetic inductance using the results obtained in Sec. III.

A. Depairing current density

For $T = 0$, the depairing current density j_d is already obtained for some Γ values (colored blobs in Fig. 5). That for an arbitrary Γ can also be calculated from the formulas, Eqs. (21)-(23), by finding the maximum values of j_s . Shown as the solid curves in Fig. 7 are j_d , q_d and $s_d = (q_d/q_\xi)^2$ as functions of Γ . An increase of Γ leads to decreases of n_s and j_s , resulting in a monotonic decrease of j_d .

For $\Gamma \ll 1$, we can derive an analytical formula for j_d . Using Eqs. (24)-(26) and the condition $\partial_s j_s = 0$, we find (see Appendix C)

$$j_d(\Gamma, 0) = \sqrt{\pi s_d} \left[\Delta_d - \frac{4s_d}{3\pi} - \frac{2\Gamma}{\pi} \right] \frac{H_{c0}}{\lambda_0}, \quad (33)$$

$$\Delta_d = \Delta_{d0} \exp \left[\left(\frac{\pi\alpha}{4} - 1 \right) \frac{\Gamma}{\Delta_{d0}} \right], \quad (34)$$

$$s_d = (s_{d0} - \alpha\Gamma) \exp \left[\left(\frac{\pi\alpha}{4} - 1 \right) \frac{\Gamma}{\Delta_{d0}} \right], \quad (35)$$

$$\zeta_{d0} = \frac{2}{\pi} + \frac{3\pi}{8} - \sqrt{\left(\frac{2}{\pi} + \frac{3\pi}{8} \right)^2 - 1} = 0.300, \quad (36)$$

$$\Delta_{d0} = e^{-\frac{\pi}{4}\zeta_{d0}} = 0.790, \quad (37)$$

$$s_{d0} = \Delta_{d0}\zeta_{d0} = 0.237, \quad (38)$$

$$\alpha = \frac{1 + \pi/2 - 2(1 + 8/\pi)\zeta_{d0}}{2 + 3\pi^2/8 - \pi\zeta_{d0}} = 0.365. \quad (39)$$

Shown as the dashed curves in Fig. 7 are calculated from Eqs. (33)-(39), which agree well with the exact results (solid curves) at $\Gamma \ll 1$. For $\Gamma = 0$, we have $\Delta_d = \Delta_{d0} = 0.790$ and $s_d = s_{d0} = 0.237$, reproducing the well-known result, $j_d(0, 0) = 0.595 H_{c0}/\lambda_0$ [13, 14, 37].

For $T \simeq T_c$, we can use Eqs. (30)-(32). The condition $\partial_s j_s = 0$ yields $s_d = s_m/3 = (4T_c/3\pi)(1 - T/T_c)$, and we have [52]

$$j_d(\Gamma, T) = \left(\frac{2}{3} \right)^{\frac{3}{2}} \frac{H_c(\Gamma, T)}{\lambda(0, \Gamma, T)} = 0.544 \frac{H_c(\Gamma, T)}{\lambda(0, \Gamma, T)}. \quad (40)$$

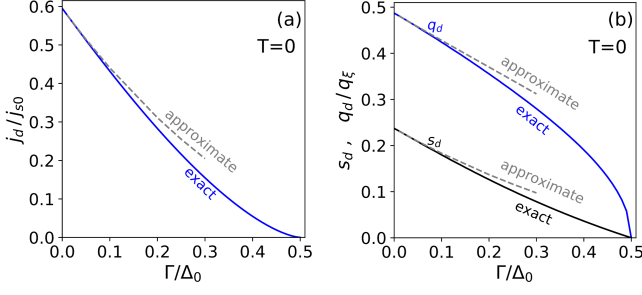


FIG. 7. (a) Depairing current density j_d at $T = 0$ as a function of Γ . (b) Depairing momentum q_d and $s_d = (q_d/q_\xi)^2$ at $T = 0$ as functions of Γ . The solid curves represent the exact results calculated from Eqs. (21)-(23). The dashed curves are calculated from the approximate formulas given by Eqs. (33)-(39).

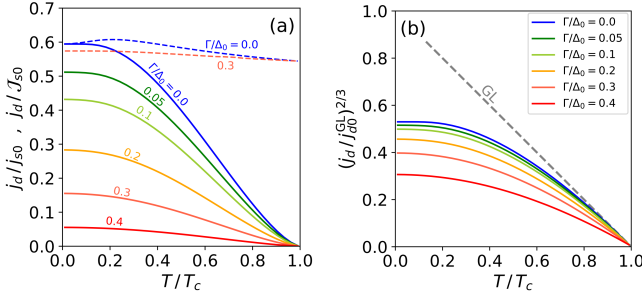


FIG. 8. (a) Depairing current density $j_d(\Gamma, T)/j_{s0}$ and $j_d(\Gamma, T)/J_{s0}(\Gamma, T)$ as functions of T/T_c for different Γ . Here $J_{s0}(\Gamma, T) = H_c(\Gamma, T)/\lambda(0, \Gamma, T)$ and $j_{s0} = J_{s0}(0, 0) = H_{c0}/\lambda_0$. (b) Depairing current density $(j_d/j_{d0}^{GL})^{2/3}$ as functions of T/T_c . Here j_{d0}^{GL} is defined by Eq. (42). The dashed gray line is the GL result [Eq. (41)] extrapolated to lower T regions.

Eq. (40) can be written as

$$j_d(\Gamma, T) = j_{d0}^{GL} \left(1 - \frac{T}{T_c} \right)^{\frac{3}{2}}, \quad (41)$$

where

$$j_{d0}^{GL} = \frac{16j_{s0}}{21\zeta(3)} \sqrt{\frac{\pi}{3}} \left(\frac{e^{\gamma_E} T_c}{T_{c0}} \right)^{\frac{3}{2}} = \frac{8\pi^2 \sqrt{2\pi}}{21\zeta(3)e} \sqrt{\frac{(k_B T_c)^3}{\hbar v_F \rho(\rho/\tau)}}, \quad (42)$$

Eqs. (40)-(42) have the same form as the well-known GL depairing current density except T_c depends on Γ through Eq. (15).

For $0 < T < T_c$, we can obtain $j_d(\Gamma, T)$ by numerically solving Eqs. (2)-(7) for different Γ and T and finding the maximum value of j_s . Shown as solid curves in Fig. 8 (a) are $j_d(\Gamma, T)$ as functions of T for different Γ . The Kupriyanov-Lukichev-Maki's result [13, 14, 35] is reproduced for the ideal BCS superconductor with

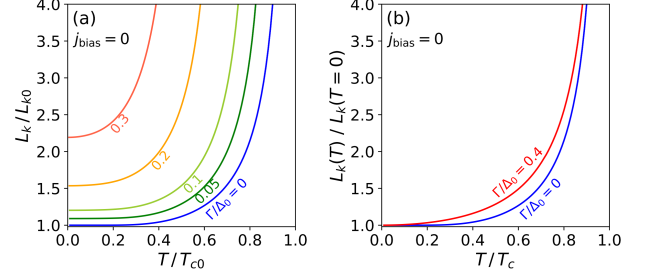


FIG. 9. Zero-current kinetic inductance $L_k(0, \Gamma, T)$ calculated from the formula given by Eq. (44). (a) $L_k(0, \Gamma, T)$ as functions of T . Here, $L_{k0} = L_k(0, 0, 0) = \mu_0 \lambda_0^2$. (b) $L_k(0, \Gamma, T)/L_k(0, \Gamma, 0)$ as functions of the normalized temperature T/T_c .

$\Gamma = 0$ (blue curve), while a finite Γ reduces j_d for all T . The dashed curves represent $j_d(\Gamma, T)/J_{s0}(\Gamma, T)$, where $J_{s0}(\Gamma, T) = H_c(\Gamma, T)/\lambda(0, \Gamma, T)$. The curves merge at $T \rightarrow T_c$ and take 0.544, consistent with Eq. (40). It is sometimes useful to plot $(j_d/j_{d0}^{GL})^{2/3}$ as functions of T/T_c (see, e.g., Refs. [65–67]). Shown as solid curves in Fig. 8 (b) are $(j_d/j_{d0}^{GL})^{2/3}$ obtained by numerically solving Eqs. (2)-(7). The dashed line represents the GL result given by Eq. (41), which is valid only at $T \simeq T_c$.

B. Kinetic inductance

The kinetic inductance of a narrow thin-film is given by $L_{\text{film}} = (\ell/Wd)L_k$ for the length ℓ , width W , and thickness d . The kinetic inductivity L_k is defined by $L_k \dot{j}_s = -\dot{A}$ [37, 68], the dot denotes differentiation with respect to the time t , and $A = \hbar q/2|e|$ is the vector potential. Hence,

$$L_k(s, \Gamma, T) = \frac{\hbar(-\dot{q}/\dot{j}_s)}{2|e|} = \mu_0 \lambda_0^2 \frac{\dot{q}}{\dot{q}_{n_{s0}} + q_{n_{s0}}}. \quad (43)$$

Here $\hbar q_\xi/2\sqrt{\pi}|e|j_{s0} = \mu_0 \lambda_0^2$ is used. In the following, we investigate L_k for the zero-current limit and the current-carrying state in the fast- and the slow-measurement regimes [37, 68] for all T , all Γ , and all j_s up to $j_d(\Gamma)$.

1. Zero-current limit ($s \rightarrow 0$)

We start from the zero-current limit. Taking $q \rightarrow 0$, Eq. (43) reduces to $L_k(0, \Gamma, T) = \mu_0 \lambda_0^2 n_{s0}/n_s(0, \Gamma, T) = \mu_0 \lambda^2(0, \Gamma, T)$. Using the analytical expression for $n_s(0, \Gamma, T)$ [50, 52], we find the general formula for the zero-current kinetic inductance,

$$L_k(0, \Gamma, T) = \frac{\mu_0 \lambda_0^2}{\frac{2\Delta(0, \Gamma, T)}{\pi} \text{Im}\psi\left[\frac{1}{2} + \frac{\Gamma + i\Delta(0, \Gamma, T)}{2\pi T}\right]}, \quad (44)$$

where $\Delta(0, \Gamma, T)$ can be calculated from Eq. (3) (see also Fig. 4). For the ideal BCS superconductor ($\Gamma = 0$), Eq. (44) reproduces the well-known result [36, 37, 69]:

$$L_k(0, 0, T) = \mu_0 \lambda_0^2 \frac{1}{\tanh \frac{\Delta(0, 0, T)}{2T}}. \quad (45)$$

For $T = 0$ and $\Gamma \geq 0$, Eq. (44) reduces to

$$L_k(0, \Gamma, 0) = \frac{\mu_0 \lambda_0^2}{\Delta(0, \Gamma, 0) \left[1 - \frac{2}{\pi} \tan^{-1} \frac{\Gamma}{\Delta(0, \Gamma, 0)} \right]}, \quad (46)$$

where $\Delta(0, \Gamma, 0)$ can be calculated from Eq. (14). At $T = \Gamma = 0$, Eqs. (45) and (46) yield

$$L_{k0} = L_k(0, 0, 0) = \mu_0 \lambda_0^2. \quad (47)$$

In the GL regime, we can use Eq. (20):

$$L_k(0, \Gamma, T) = \frac{7\zeta(3)\mu_0\lambda_0^2}{4\pi^2 T_c} \left(1 - \frac{T}{T_c} \right)^{-1}. \quad (48)$$

for $T \simeq T_c$.

Shown in Fig. 9 (a) are L_k in the zero-current state as functions of T for different Γ calculated from Eq. (44). As T or Γ increase, the superfluid density n_s decreases, and L_k increases and diverges at $T = T_c$ or $\Gamma = 1/2$. Shown in Fig. 9 (b) are $L_k(0, \Gamma, T)$ normalized with $L_k(0, \Gamma, T)|_{T=0}$ as functions of $T/T_c(\Gamma)$. The blue curve, which represents the ideal BCS superconductor with $\Gamma = 0$, obeys Eq. (45). The red curve ($\Gamma = 0.4$) represents a superconductor with large densities of subgap states (see also Fig. 1), which grows up with T/T_c faster the ideal one.

2. Current carrying state ($s > 0$): Fast measurement

Now consider a current-carrying superconductor in the fast measurement regime [37, 68], in which the time-dependent current changes rapidly about its time average on a time scale much shorter than the relaxation time of n_s . We assume n_s cannot follow the time dependence of the current and take $\dot{n}_s \rightarrow 0$. Then, Eq. (43) reduces to

$$L_k(s, \Gamma, T) = \mu_0 \lambda_0^2 \frac{n_{s0}}{n_s(\langle s \rangle, \Gamma, T)} = \mu_0 \lambda^2(\langle s \rangle, \Gamma, T), \quad (49)$$

where $\langle s \rangle$ is the time average of $s(t)$. Experiments in this regime is found in e.g., Ref. [69].

We consider a superconductor under a dc biased rf current: $q(t) = q_{\text{bias}} + q_{\text{rf}}(t)$, $s(t) = [q(t)/q_\xi]^2 = s_{\text{bias}} + s_{\text{rf}}(t)$, and $j_s = j_s(s_{\text{bias}} + s_{\text{rf}}(t)) = j_{\text{bias}} + j_{\text{rf}}(t)$. In this case, we have $\langle s \rangle = s_{\text{bias}} = (q_{\text{bias}}/q_\xi)^2$ and $j_{\text{bias}} = j_s(s_{\text{bias}})$. Note that, when $s_{\text{bias}} = 0$, Eq. (49) reduces to the zero-current kinetic inductance, Eq. (44).

For $T = 0$, we can use Eqs. (21)-(23) to evaluate Eq. (49). Shown in Fig. 10 (a) are $L_k(j_{\text{bias}}, \Gamma, T)|_{T=0}$ as functions of the dc bias current j_{bias} for different Γ . As j_{bias} increases, L_k monotonically increases and reaches the maximum at the depairing current density j_d (colored blob). Shown in Fig. 10 (b) are $L_k(j_{\text{bias}}, \Gamma, 0)$ as

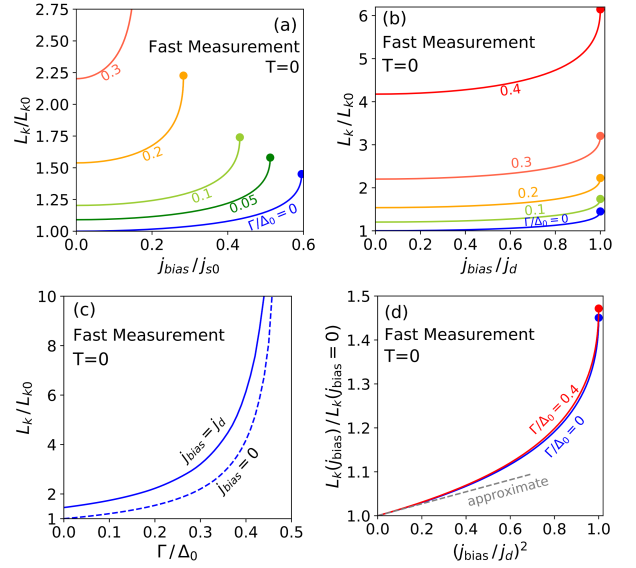


FIG. 10. Fast-measurement kinetic inductance $L_k(j_{\text{bias}}, \Gamma, T)|_{T=0}$ calculated from the formulas given by Eqs. (21)-(23) and (49). (a) $L_k(j_{\text{bias}}, \Gamma, T)|_{T=0}$ as functions of j_{bias} . (b) $L_k(j_{\text{bias}}, \Gamma, T)|_{T=0}$ as functions of $j_{\text{bias}}/j_d(\Gamma)$. (c) $L_k(j_{\text{bias}}, \Gamma, T)|_{T=0}$ as functions of Γ for $j_{\text{bias}} = 0$ (dashed curve) and $j_{\text{bias}} = j_d$ (solid curve). (d) $L_k(j_{\text{bias}}, \Gamma, 0)/L_k(0, \Gamma, 0)$ as functions of $(j_{\text{bias}}/j_d)^2$. The dashed gray line is calculated from the approximate formulas given by Eq. (50).

functions of the normalized current j_{bias}/j_d . The effects of Γ are significant rather than those of j_{bias} . Shown in Fig. 10 (c) are $L_k(j_{\text{bias}}, \Gamma, 0)$ as functions of Γ for $j_{\text{bias}} = 0$ (dashed curve) and $j_{\text{bias}} = j_d$ (solid curve). While both the curves quickly increase with Γ and diverge at $\Gamma = 1/2$, the difference between the solid and dashed curves is always smaller than factor 1.5. Shown in Fig. 10 (d) are $L_k(j_{\text{bias}}, \Gamma, 0)/L_k(0, \Gamma, 0)$ as functions of $(j_{\text{bias}}/j_d)^2$ for different Γ . The blue ($\Gamma = 0$) and red ($\Gamma = 0.4$) curves almost overlap, and the effects of j_{bias} is less than 1.5 independent of Γ . It should be noted that the blue curves in Figs. 10 (a), 10 (b), and 10 (d), which represent the ideal BCS superconductor with $\Gamma = 0$, are coincident with the results in the previous study [37].

To understand the nonlinear L_k for small current regions, we use the approximate formulas, Eqs. (27)-(29). After some calculations, we find (see Appendix D):

$$L_k(j_{\text{bias}}, \Gamma, 0) = L_k(0, \Gamma, 0) \left[1 + C_{\text{fm}} \left(\frac{j_{\text{bias}}}{j_d} \right)^2 \right], \quad (50)$$

$$C_{\text{fm}} = \frac{(3\pi^2 + 16)s_{d0}}{12\pi} \left(\Delta_{d0} - \frac{4s_{d0}}{3\pi} \right)^2 = 0.136, \quad (51)$$

for $T = 0$ and $(j_{\text{bias}}/j_d)^2 \ll 1$. Here Δ_{d0} and s_{d0} are given by Eqs. (37) and (38). Shown as the dashed gray line in Fig. 10 (d) is calculated from Eq. (50), which agrees well with the exact results (solid curves) at $(j_{\text{bias}}/j_d)^2 \ll 1$.

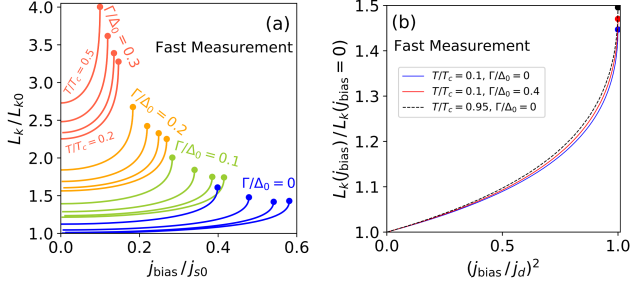


FIG. 11. Fast measurement kinetic inductance $L_k(j_{\text{bias}}, \Gamma, T)$ for a finite T . (a) $L_k(j_{\text{bias}}, \Gamma, T)$ as functions of j_{bias} up to j_d calculated for $\Gamma = 0, 0.1, 0.2, 0.3$ and $T/T_c = 0.2, 0.3, 0.4, 0.5$. The colored blobs are the depairing points. (b) $L_k(j_{\text{bias}}, \Gamma, T)/L_k(0, \Gamma, T)$ as functions of $(j_{\text{bias}}/j_d)^2$ for $T/T_c = 0, 0.95$ and $\Gamma = 0, 0.4$.

For $T \simeq T_c$, Eq. (49) can be calculated from Eqs. (30)-(32). Hence,

$$L_k(s_{\text{bias}}, \Gamma, T) = \frac{7\zeta(3)\mu_0\lambda_0^2}{4\pi^2 T_c} \left(1 - \frac{T}{T_c}\right)^{-1} \left(1 - \frac{s_{\text{bias}}}{3s_d}\right)^{-1} \\ = L_k(0, \Gamma, T) \left(1 - \frac{s_{\text{bias}}}{3s_d}\right)^{-1}, \quad (52)$$

for $T \simeq T_c$. Here $s_d = s_m/3 = (4T_c/3\pi)(1 - T/T_c)$ and Eq. (48) are used. When $s_{\text{bias}} = s_d$, we have $L_k(s_d, \Gamma, T)/L_k(0, \Gamma, T)|_{T \simeq T_c} = 1.5$. The bias momentum parameter s_{bias} can be converted to j_{bias}/j_d by using Eqs. (32) and (40). For small current regions, we have $s_{\text{bias}}/3s_d = (4/27)(j_{\text{bias}}/j_d)^2$ and obtain

$$L_k(j_{\text{bias}}, \Gamma, T) = L_k(0, \Gamma, T) \left[1 + C_{\text{fm}}^{\text{GL}} \left(\frac{j_{\text{bias}}}{j_d}\right)^2\right], \quad (53)$$

$$C_{\text{fm}}^{\text{GL}} = \frac{4}{27} = 0.148, \quad (54)$$

for $T \simeq T_c$ and $(j_{\text{bias}}/j_d)^2 \ll 1$. Eq. (53) has the same form as that obtained in the previous study [68] except T_c and j_d depend on Γ . Note the value of $C_{\text{fm}}^{\text{GL}}$ differs from that of C_{fm} at $T = 0$.

For $0 < T < T_c$, we use the numerical solutions of Eqs. (2)-(7). Shown in Fig. 11 (a) are $L_k(j_{\text{bias}}, \Gamma, T)$ as functions of j_{bias} for different Γ and T . The blobs represent the depairing points. Shown in Fig. 11 (b) are $L_k(j_{\text{bias}}, \Gamma, T)/L_k(0, \Gamma, T)$ for different Γ and T , which are not sensitive neither to Γ nor T/T_c [see also Fig. 10 (d) for $T = 0$]. The similar curves for $\Gamma = 0$ are found in Ref. [37].

3. Current carrying state ($s > 0$): Slow measurement

Consider the other limit, the slow measurement regime [37, 68], in which the time-dependent current changes on a time scale much longer than the relaxation

time of n_s . In this case, we can assume n_s instantly follows the time dependence of the current: $n_s = n_s(q(t))$. Substituting $\dot{n}_s = \dot{q}\partial_q n_s$ into Eq. (43), we find

$$L_k(s, \Gamma, T) = \mu_0\lambda_0^2 \left[(1 + q\partial_q) \frac{n_s(s, \Gamma, T)}{n_{s0}} \right]^{-1} \quad (55)$$

$$= \mu_0\lambda_0^2 \sqrt{\pi} \left| \frac{\partial(j_s/j_{s0})}{\partial(q/q_\xi)} \right|^{-1}, \quad (56)$$

where Eq. (56) corresponds with the expression given in Ref. [37].

For $T = 0$, we can evaluate Eq. (56) using the solutions of Eqs. (21)-(23). Shown in Fig. 12 (a) are $L_k(j_s, \Gamma, T)|_{T=0}$ as functions of j_s , which diverge at $j_s = j_d(\Gamma)$. These divergences come from $\partial_q j_s = 0$ at $j_s = j_d$ (see also Fig. 5). Shown in Fig. 12 (b) are $L_k(j_s, \Gamma, 0)/L_k(0, \Gamma, 0)$ as functions of the normalized current $(j_s/j_d)^2$, which are not sensitive to Γ .

For small-current regions, we have an useful formula to calculate L_k (see Appendix D):

$$L_k(j_s, \Gamma, 0) = L_k(0, \Gamma, 0) \left[1 + C_{\text{sm}} \left(\frac{j_s}{j_d}\right)^2\right], \quad (57)$$

$$C_{\text{sm}} = \frac{(3\pi^2 + 16)s_{d0}}{4\pi} \left(\Delta_{d0} - \frac{4s_{d0}}{3\pi}\right)^2 = 0.544, \quad (58)$$

for $T = 0$ and $(j_s/j_d)^2 \ll 1$. Hence, we have a relation $C_{\text{sm}} = 4C_{\text{fm}}$ [see Eqs. (53) and (54)]. Shown as the dashed gray line in Fig. 12 (b) is the normalized L_k calculated from Eq. (57), which agrees well with the exact results (solid curves) at $(j_s/j_d)^2 \ll 1$.

For $T \simeq T_c$, we use the GL results. Substituting Eq. (32) into Eq. (56), we obtain

$$L_k(s, \Gamma, T) = L_k(0, \Gamma, T) \left(1 - \frac{s}{s_d}\right)^{-1}. \quad (59)$$

When $s \ll s_d$, we have $s/s_d = (4/9)(j_s/j_d)^2$ and obtain

$$L_k(s, \Gamma, T) = L_k(0, \Gamma, T) \left[1 + C_{\text{sm}}^{\text{GL}} \left(\frac{j_s}{j_d}\right)^2\right], \quad (60)$$

$$C_{\text{sm}}^{\text{GL}} = \frac{4}{9} = 0.444, \quad (61)$$

for $T \simeq T_c$ and $(j_s/j_d)^2 \ll 1$. We find C_{sm} for $T \simeq T_c$ is smaller than that at $T = 0$. Eq. (60) has the same form as the well-known result [68] except T and j_d depend on Γ .

For $0 < T < T_c$, we use the numerical solutions of Eqs. (2)-(7). Shown in Fig. 13 (a) are $L_k(j_s, \Gamma, T)$ as functions of j_s for different Γ and T , which increase with j_s and diverge at $j_s = j_d(\Gamma)$, $\Gamma = 1/2$, and $T = T_c(\Gamma)$. Shown in Fig. 13 (b) are $L_k(j_s, \Gamma, T)/L_k(0, \Gamma, T)$ as functions of $(j_s/j_d)^2$ for different Γ and T , sensitive neither to Γ nor T . This insensitivity resembles that for the fast measurement case [see also Fig. 11 (b)]. See also Ref. [37] for $\Gamma = 0$.

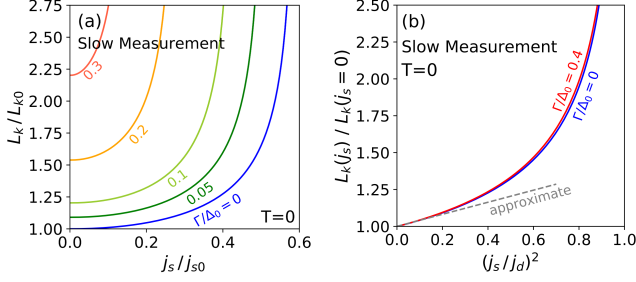


FIG. 12. Slow-measurement kinetic inductance $L_k(j_s, \Gamma, T)|_{T=0}$ calculated from the formulas given by Eqs. (21)-(23) and (56). (a) L_k as functions of j_s . (b) L_k normalized with $L_k(j_s = 0)$ as functions of $(j_s/j_d)^2$. The dashed gray line is calculated from the approximate formulas given by Eq. (57).

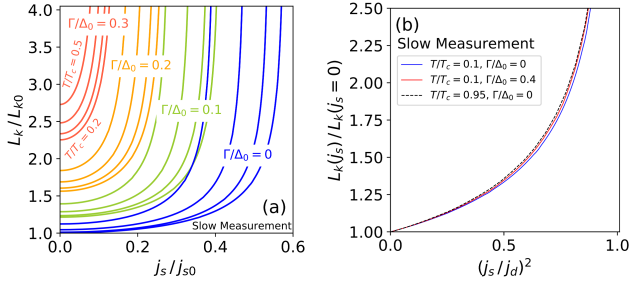


FIG. 13. (a) Slow-measurement kinetic inductance $L_k(j_s, \Gamma, T)$ at finite temperatures as functions of j_s up to j_d calculated for $\Gamma = 0, 0.1, 0.2, 0.3$ and $T/T_c = 0.2, 0.3, 0.4, 0.5$. (b) $L_k(j_s, \Gamma, T)/L_k(0, \Gamma, T)$ as functions of $(j_s/j_d)^2$ for $\Gamma = 0, 0.4$ and $T/T_c = 0.1, 0.95$.

V. SEMI-INFINITE SUPERCONDUCTOR

In this section, we consider the geometry shown in Fig. 2 (b): a semi-infinite superconductor occupying $x \geq 0$. We calculate the current distribution and the superheating field.

A. Current distribution

In the Meissner state, the current distributes within the depth $\sim \lambda$ from the surface. When the superfluid flow is small ($|q| \ll q_d$), the pair-breaking effect due to a finite q is negligible, and the distributions of the current $j_s(x)$ and the magnetic field $H(x)$ obey the London equation. As $|q|$ increases, the London equation ceases to be valid due to the current-induced pair-breaking effect (nonlinear Meissner effect [17, 70]). To obtain the current and field distributions, we need the self-consistent solutions of the coupled Maxwell and Usadel equations, Eqs. (2)-(10).

Let us consider the simplest case: $T = 0$ and $\Gamma = 0$. For $H_0 \rightarrow 0$, we can use the London equation, which

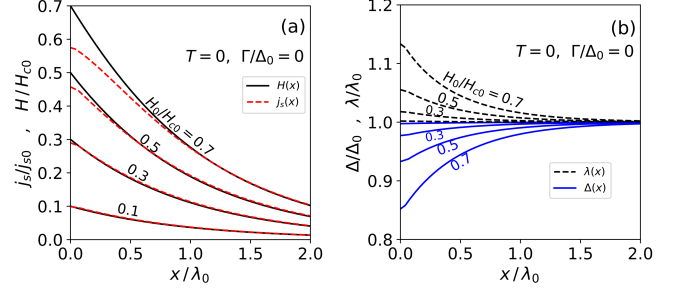


FIG. 14. Distributions of (a) H , j_s , (b) Δ , and λ in the semi-infinite superconductor for the surface magnetic field $H_0/H_{c0} = 0.1, 0.3, 0.5, 0.7$.

gives $H(x)/H_{c0} = j_s(x)/j_{s0} = H_0/H_{c0} \exp(-x/\lambda_0)$: the curves for $H(x)/H_{c0}$ and $j_s(x)/j_{s0}$ completely overlap. Shown in Fig. 14 (a) are $H(x)$ and $j_s(x)$ as functions of x for different H_0 calculated from the self-consistent solutions of Eqs. (2)-(10). For small H_0 regions, in fact, $H(x)/H_{c0}$ (solid curves) and $j_s(x)/j_{s0}$ (dashed curves) almost overlap, expected from the London equation. However, as H_0 increases, the dashed curves deviate from the solid curves in the vicinity of the surface: the non-linear Meissner effect manifests itself. Shown in Fig. 14 (b) are $\Delta(x)$ and $\lambda(x)$, which differ from the zero-current values (Δ_0 and λ_0) at $x \lesssim \lambda$ but approach Δ_0 and λ_0 as x increases.

B. Superheating field

The superheating field H_{sh} is given by the value of H_0 which induces $j_s(x_0) = j_d$. Here x_0 is the depth at which the distribution $j_s(x)$ takes the maximum. Note here it is not necessarily the case that we have $x_0 = 0$. For instance, in the multilayer structure [11, 51, 71–73] or a superconductor including inhomogeneous impurities in the vicinity of the surface [11, 41, 51], the surface current can be suppressed, and $j_s(x)$ takes the maximum at the inside ($x_0 > 0$).

In our semi-infinite superconductor, the current is a monotonically decreasing function of x as shown in Fig. 14 (a). Hence, $x_0 = 0$. In this case, we can derive a simple formula of H_{sh} . Integrating both the sides of Eq. (8) from $x = 0$ to ∞ , we obtain $q'(0)^2 = -2 \int_0^\infty q q' \lambda^{-2}(s, \Gamma, T) dx$. Then, Using Eqs. (9) and (10), we find the relation between the applied magnetic field H_0 and the superfluid flow at the surface $s(0)$:

$$\frac{H_0^2}{H_{c0}^2} = \int_0^{s(0)} \frac{\pi \lambda_0^2 ds}{\lambda^2(s, \Gamma, T)} = \pi \int_0^{s(0)} ds \frac{n_s(s, \Gamma, T)}{n_{s0}}. \quad (62)$$

H_{sh} can be calculated by substituting $s(0) = s_d$:

$$H_{sh}(\Gamma, T) = H_{c0} \sqrt{\pi \int_0^{s_d(\Gamma, T)} ds \frac{n_s(s, \Gamma, T)}{n_{s0}}}, \quad (63)$$

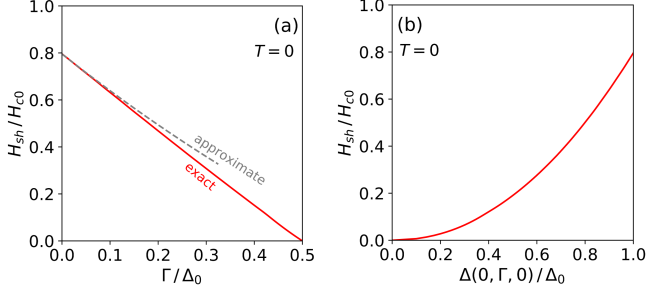


FIG. 15. Superheating field $H_{sh}(\Gamma, T)$ at $T = 0$. (a) H_{sh} as a function of Γ . The dashed curve is calculated from the approximate formula given by Eqs. (64)-(66). (b) H_{sh} as a function of Δ in the zero-current state.

which is the general formula of the superheating field for a homogeneous dirty superconductor, valid for arbitrary Γ and T .

For $T = 0$, we can evaluate Eq. (63) by using Eqs. (21) and (22) [see also Figs. 5 (b) and 7 (b)]. Shown as the solid red curve in Fig. 15 (a) is $H_{sh}(\Gamma, T)|_{T=0}$ as a function of Γ . As Γ increases, H_{sh} decreases and vanishes at $\Gamma = 1/2$. Shown in Fig. 15 (b) is $H_{sh}(\Gamma, 0)$ as a function of $\Delta(0, \Gamma, 0)/\Delta(0, 0, 0)$.

For $T = 0$ and $\Gamma \ll 1$ (such that $\Gamma \ll \Delta - s$, Eq. (63) reduces to a formula (see Appendix E),

$$H_{sh}(\Gamma, 0) = H_{c0} \sqrt{I(\Gamma) - \frac{2}{3}s_d^2(\Gamma) - 2\Gamma s_d(\Gamma)}, \quad (64)$$

where

$$I(\Gamma) = 1 - \left(1 - \frac{\pi z_d}{2}\right) e^{-\frac{\pi z_d}{2}} - 4\Gamma(1 - e^{-\frac{\pi z_d}{4}}), \quad (65)$$

$$z_d(\Gamma) = \zeta_d \frac{1 - \frac{\pi}{4}\zeta_d}{1 - \frac{\pi}{4}\zeta_d + \frac{\Gamma}{\Delta_d}}, \quad (66)$$

$\zeta_d = s_d/\Delta_d$ and s_d are given by Eqs. (34) and (35). For the ideal dirty BCS superconductor ($\Gamma = 0$), we have $z_d = \zeta_{d0}$ and

$$\begin{aligned} H_{sh}(0, 0) &= H_{c0} \sqrt{1 - \left(1 - \frac{\pi \zeta_{d0}}{2}\right) e^{-\frac{\pi \zeta_{d0}}{2}} - \frac{2}{3}s_{d0}^2} \\ &= 0.79H_{c0}. \end{aligned} \quad (67)$$

This is slightly smaller than the clean-limit value, $H_{sh}^{\text{clean}}(0, 0) = 0.84H_{c0}$ [38, 39], and is consistent with the previous study [40], in which H_{sh} takes the maximum at the mean free path (mfp) = $5.32\xi_0$ and decreases with mfp.

For $T \simeq T_c$, we use the GL results. Substituting Eqs. (30) and (31) into Eq. (63) and using the depairing value of the s parameter in the GL regime, $s_d(\Gamma, T) = s_m/3 = (4T_c/3\pi)(1 - T/T_c)$, we obtain

$$H_{sh}(\Gamma, T)|_{T \simeq T_c} = \frac{\sqrt{5}}{3}H_c(\Gamma, T) = 0.745H_c(\Gamma, T). \quad (68)$$

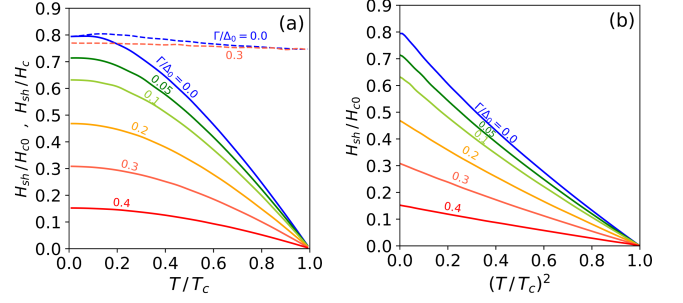


FIG. 16. Superheating field $H_{sh}(\Gamma, T)$ at finite temperatures. (a) $H_{sh}(\Gamma, T)/H_{c0}$ (solid curves) and $H_{sh}(\Gamma, T)/H_c(\Gamma, T)$ (dashed curves) as functions of T/T_c for different Γ . (b) H_{sh} as functions of $(T/T_c)^2$.

The coefficient is independent of Γ and coincident with the well-known GL result obtained for $\Gamma = 0$ [74, 75].

For $0 < T < T_c$, we use the numerical solutions of $n_s(s, \Gamma, T)$ and $s_d(\Gamma, T)$ [see Fig. 6 (b)]. Shown as the solid curves in Fig. 16 (a) is $H_{sh}(\Gamma, T)$ as functions of T/T_c . We find H_{sh} is a monotonically decreasing function of Γ and T . Shown as the dashed curves in Fig. 16 (a) is $H_{sh}(\Gamma, T)$ normalized by $H_c(\Gamma, T)$. The curves merge at $T \rightarrow T_c$ and reproduce the GL coefficient $\sqrt{5}/3$. It is often useful to plot H_{sh} as functions of $(T/T_c)^2$ (see, e.g., Ref. [28]). Shown in Fig. 16 (b) is H_{sh} as functions of $(T/T_c)^2$. The slope of H_{sh} is steeper than $[1 - (T/T_c)^2]$ decreases as Γ increases.

VI. DISCUSSIONS

In Sec. III, we have investigated a disordered superconductor with a finite Dynes Γ parameter by solving the Usadel equation. We have calculated $\Delta(s, \Gamma, T)$, $n_s(s, \Gamma, T)$, $\lambda(s, \Gamma, T)$, and $j_s(s, \Gamma, T)$ for all T , all Γ , and all superfluid flow parameter $s \propto q^2$. Besides, we have derived the formulas of Δ , n_s , λ , and j_s at $T = 0$, taking the effects of Γ into account [Eqs. (21)-(29)]. The formulas for $T \simeq T_c$ have also been obtained, which have the similar forms as the usual GL results except that T_c depends on Γ . Using these results, we have investigated a narrow thin-film in Sec. IV and a semi-infinite superconductor in Sec. V. In the following, we summarize the results and discuss their implications.

A. Depairing current density

In Sec. IV A, we have calculated the depairing current density $j_d(\Gamma, T)$ for all T and all Γ (see Fig. 8). Also, we have derived the analytical formulas for j_d valid for $T = 0$ and $\Gamma \ll 1$ [see Eqs. (33)-(39)]. The formulas for $T \simeq T_c$ has the similar form as the well-known GL depairing current except that T_c depends on Γ [see Eqs. (40)-(42)].

Our results show that j_d is given by the Kupriyanov-Lukichev-Maki (KLM) theory for $\Gamma = 0$ and decreases as Γ increases. Hence, we can expect that real materials, which usually have $\Gamma > 0$, exhibit smaller j_d than the ideal KLM value. The previous measurements do not contradict this expectation, but the correlation between j_d and Γ is still unclear. Simultaneous measurements of j_d and Γ can provide with a deeper insight into observed values of j_d .

While materials mechanisms behind Γ are not well-understood, it would be possible to engineer Γ by combining tunnel measurements and various materials processing. Finding a better materials processing method which can reduce Γ , we can ameliorate j_d .

In SNSPD, the detection efficiency (DE) depends on the bias current j_{bias}/j_d . Then, an increase or decrease of j_d via a Γ engineering (see Fig. 7) would result in a shift of the necessary dc bias. For instance, when $\Gamma = 0.1$, we have more than 10% degradation of T_c and 30% degradation of j_d compared with the ideal BCS superconductor, which would reduce the necessary dc bias by 30%. Simultaneous measurements of Γ , j_d and DE before and after materials treatments (e.g., ion irradiation [76]) can test the theory.

B. Kinetic inductance

In Sec. IV B 1, we have derived the zero-current kinetic inductance formula, Eq. (44). By using this formula, we have calculated $L_k(0, \Gamma, T)$ for all T and all Γ . Our results show that Γ affects the T dependence of $L_k(0, \Gamma, T)/L_k(0, \Gamma, 0)$ as shown in Fig. 9 (b). Simultaneous measurements of Γ and the zero-current kinetic inductance for different T can confirm the theoretical prediction.

In Sec. IV B 2 and Sec. IV B 3, we have numerically calculated the current dependent nonlinear kinetic inductance in the fast- and the slow-measurement regimes for all T , all Γ , and all current up to j_d (see Figs. 11 and 13). In the fast measurement regime, the current-induced increase of $L_k(j_{\text{bias}}, \Gamma, T)/L_k(0, \Gamma, T)$ is at most ~ 1.5 even at j_d . The coefficient of the quadratic expansion at $T = 0$ is $C_{\text{fm}} = 0.136$ [see Eqs. (50)]. On the other hand, in the slow measurement regime, L_k diverges at j_d , and the coefficient of the quadratic expansion at $T = 0$ is given by $C_{\text{sm}} = 4C_{\text{fm}} = 0.544$ [see Eqs. (57)]. The difference between the fast- and the slow-measurement results would be detectable in experiments. The effects of Γ on C_{fm} and C_{sm} are not significant. To test the theory, measurements of the current-dependent nonlinear kinetic inductance should be combined with a measurement of j_d and tunneling spectroscopy to extract Γ .

Also, our theory suggests that it would be possible to tune L_k by engineering Γ as well as by the dc or ac current and controlling T . While L_k always increases with the bias current and Γ , the dissipative conductivity σ_1 can be smaller than that of the ideal BCS superconductor

by tuning the dc bias and Γ (see Fig. 7 in Ref. [52]). Then, we can simultaneously increase L_k and reduce σ_1 (e.g., $\Gamma = 0.05$ and $j_s \ll j_d$ lead to 10% increase of L_k and 20% reduction of σ_1 [9, 50, 52]). These results might be useful for developing superconducting circuit elements (e.g., superinductor [77]).

C. Superheating field

In Sec. V, we have derived the general formula of the superheating field for a disordered superconductor H_{sh} , taking the effects of Γ into account [see Eq. (63)]. Using this formula, we have calculated $H_{sh}(\Gamma, T)$ for all T and all Γ . A simple analytical formula for $T = 0$ and $\Gamma \ll 1$ is also derived, which is given by Eq. (64). For the ideal dirty BCS superconductor with $\Gamma = 0$, we have obtained $H_{sh}(0, 0) = 0.79H_{c0}$ at $T = 0$, which is slightly smaller than $H_{sh}^{\text{clean}} = 0.84H_{c0}$ for a clean limit superconductor with a large λ/ξ [38, 39] and consistent with the previous study [40] in which H_{sh} decreases with mfp when $\text{mfp} < 5.32\xi_0$.

According to our results, we can expect that the maximum operating field of an SRF cavity made from a homogeneous dirty BCS superconductor with $\Gamma = 0$ is given by $H_{sh}(0, 0) = 0.79H_{c0}$. Taking dirty Nb materials for example, $\mu_0 H_{c0} = 200$ mT yields $\mu_0 H_{sh}(0, 0) = 160$ mT, which translates into the accelerating field $E_{\text{acc}} = 37$ MV/m for the Tesla-shape SRF cavity. This can be tested by measuring quench fields of impurity-doped dirty Nb cavities with $\text{mfp} \ll \xi$. It should be noted that H_{sh} can increase as impurities decreases [40], then materials with $\text{mfp} \sim \xi$ [30–34] can have slightly higher H_{sh} than $0.79H_{c0}$.

Strong local-heating (and resultant quenches) of SRF cavities are often attributed to geometrical defects on the surface [78–86]. Our theory suggest there can be another source of local heating. Since real materials have a finite Γ [43, 44] and $H_{sh}(\Gamma, 0) < H_{sh}(0, 0)$, an area with a large Γ on the inner surface can be a hot spot even when $H_0 \ll H_{sh}(0, 0)$. For instance, H_{sh} at an area with $\Gamma = 0.3$ on the surface of Nb₃Sn can be estimated as $\mu_0 H_{sh} = 160$ mT at $T = 0$ from Fig. 15, which is much smaller than the ideal value $\mu_0 H_{sh}(0, 0) = 430$ mT. Here $\mu_0 H_{c0} = 540$ mT is used. Taking another example, H_{sh} at an area with $\Gamma = 0.15$ on the surface of disordered Nb materials can be estimated as $\mu_0 H_{sh} = 110$ mT at $T = 0$, which is smaller than the ideal dirty Nb by 30%. Such an area with $\Gamma > 0$ can be a source of local heating and may cause quenches. Simultaneous measurements of an onset field of local heating and Γ at the hot spot can test the theory. Materials processing that can reduce Γ would improve the accelerating field of SRF cavities.

The multilayer structure [11, 51, 71–73] or a superconductor including inhomogeneous impurities in the vicinity of the surface [11, 41, 51] can suppress the surface current and enhance H_{sh} . The formula of H_{sh} given by Eq. (63) is not applicable to these structure because $j_s(x)$

takes the maximum at the inside ($x_0 > 0$). Study on effects of Γ on H_{sh} in these structures would be useful for comparison of the theory and experiments [87–100].

ACKNOWLEDGMENTS

I would like to express the deepest appreciation to Alex Gurevich for his hospitality during my visit to Old Dominion University. This work was supported by Japan Society for the Promotion of Science (JSPS) KAKENHI Grants No. JP17H04839, No. JP17KK0100, and JP19H04395.

Appendix A: Derivations of Eqs. (14), (16), and (17)

The θ parameter of the Matsubara Green's function for the zero-current state is given by

$$u = \cot \theta = \frac{\omega_n + \Gamma}{\Delta}. \quad (\text{A1})$$

Then the self-consistency equation at $T = 0$ can be written as

$$\begin{aligned} 0 &= \lim_{M \rightarrow \infty} \left[\int_{\Gamma/\Delta}^{(M+\Gamma)/\Delta} \frac{du}{\sqrt{1+u^2}} - \int_0^M \frac{d\omega}{\sqrt{\omega^2+1}} \right] \\ &= \lim_{M \rightarrow \infty} \left(\sinh^{-1} \frac{M+\Gamma}{\Delta} - \sinh^{-1} M - \sinh^{-1} \frac{\Gamma}{\Delta} \right) \\ &= -\ln \Delta - \sinh^{-1} \frac{\Gamma}{\Delta}, \end{aligned} \quad (\text{A2})$$

resulting in Eq. (14). Here, the Matsubara sum $2\pi T \sum_{\omega_n}$ is replaced with integration $\lim_{M \rightarrow \infty} \int_0^M d\omega$, and $d\omega = \Delta du$ and $\sinh^{-1} M = \ln M$ ($M \rightarrow \infty$) are used.

The thermodynamic critical field can be calculated from Eqs. (4) and (5). At $T = 0$, we find

$$\begin{aligned} \Omega(0, \Gamma, 0) &= -N_0 \Delta^2 \lim_{M \rightarrow \infty} \int_{\Gamma/\Delta}^{(M+\Gamma)/\Delta} du \left[\frac{1}{\sqrt{1+u^2}} \right. \\ &\quad \left. + \frac{2u^2}{\sqrt{1+u^2}} - 2u \right] \\ &= -N_0 \Delta^2 \lim_{M \rightarrow \infty} \left[-u^2 + u\sqrt{1+u^2} \right]_{\Gamma/\Delta}^{(M+\Gamma)/\Delta} \\ &= -\frac{1}{2} N_0 \Delta^2 \left(1 + \frac{2\Gamma^2}{\Delta^2} - \frac{2\Gamma}{\Delta} \sqrt{1 + \frac{\Gamma^2}{\Delta^2}} \right), \end{aligned} \quad (\text{A3})$$

resulting in Eq. (16).

The superfluid density can be calculated from Eq. (6). At $T = 0$, we have

$$\begin{aligned} \frac{n_s(0, \Gamma, 0)}{n_{s0}} &= \frac{\lambda_0^2}{\lambda^2(0, \Gamma, 0)} = \frac{2}{\pi} \int_0^\infty \frac{d\omega}{1+u^2} \\ &= \frac{2\Delta}{\pi} \int_{\Gamma/\Delta}^\infty \frac{du}{1+u^2} = \Delta \left(1 - \frac{2}{\pi} \tan^{-1} \frac{\Gamma}{\Delta} \right), \end{aligned} \quad (\text{A4})$$

namely, Eq. (17).

Appendix B: Derivations of Eqs. (21) and (22)

Generalizing the procedures in Appendix A, we can derive Eqs. (21) and (22). The Matsubara Green's function $u = \cot \theta$ for the current carrying state satisfies

$$\left(1 - \frac{\zeta}{\sqrt{1+u^2}} \right) u = \frac{\omega_n + \Gamma}{\Delta} \quad (\text{B1})$$

where $\zeta = s/\Delta$. The self-consistency equation at $T = 0$ is given by

$$\begin{aligned} 0 &= \int_0^\infty d\omega \left(\frac{1}{\Delta \sqrt{1+u^2}} - \frac{1}{\sqrt{\omega^2+1}} \right) \\ &= \int_{u_0}^\infty du \left(1 - \frac{\zeta}{(1+u^2)^{3/2}} \right) \left(\frac{1}{\sqrt{1+u^2}} - \frac{1}{\sqrt{\Delta^{-2} + [(1 - \zeta/\sqrt{1+u^2})u - \Gamma/\Delta]^2}} \right) \\ &= -\ln \Delta - \sinh^{-1} u_0 - \frac{\zeta}{2} \left(\frac{\pi}{2} - \tan^{-1} u_0 - \frac{u_0}{1+u_0^2} \right) \end{aligned} \quad (\text{B2})$$

resulting in Eq. (21). Here $u_0(s, \Gamma)$ is defined by $(1 - \zeta/\sqrt{1+u_0^2})u_0 = \Gamma/\Delta$.

The superfluid density can be calculated from Eq. (6). At $T = 0$, we find

$$\begin{aligned} \frac{n_s(s, \Gamma, 0)}{n_{s0}} &= \frac{\lambda_0^2}{\lambda^2(s, \Gamma, 0)} = \frac{2}{\pi} \int_0^\infty \frac{d\omega}{1+u^2} \\ &= \frac{2\Delta}{\pi} \int_{u_0}^\infty du \left(\frac{1}{1+u^2} - \frac{\zeta}{(1+u^2)^{3/2}} + \frac{\zeta u^2}{(1+u^2)^{5/2}} \right) \\ &= \Delta \left[1 - \frac{2}{\pi} \tan^{-1} u_0 - \frac{4\zeta}{3\pi} \left\{ 1 - \frac{u_0(3+2u_0^2)}{2(1+u_0^2)^{3/2}} \right\} \right]. \end{aligned} \quad (\text{B3})$$

This is Eq. (22).

Appendix C: Derivations of Eqs. (33)-(39)

For $\Gamma \ll \Delta(s, \Gamma, 0) - s$, we can calculate j_s from Eqs. (24)-(26), which takes the maximum when $\partial j_s / \partial s = 0$:

$$\left(\frac{\pi}{4} - \zeta_d - \frac{\Gamma}{2\Delta_d} \right) \left(1 - \frac{\pi}{4} \zeta_d - \frac{\Gamma}{\Delta_d} \right) = \frac{\pi^2}{8} \zeta_d, \quad (\text{C1})$$

$$\Delta_d = \exp \left[-\frac{\pi \zeta_d}{4} - \frac{\Gamma}{\Delta_d} \right], \quad (\text{C2})$$

$$\zeta_d = s_d / \Delta_d. \quad (\text{C3})$$

Here $\partial \Delta / \partial s = -(\pi/4)[1 - (\pi/4)(s/\Delta) - \Gamma/\Delta]^{-1}$ is used. Then the maximum value of j_s is given by

$$j_d(\Gamma, T)|_{T \rightarrow 0} = \sqrt{\pi s_d} \left[\Delta_d - \frac{4s_d}{3\pi} - \frac{2\Gamma}{\pi} \right] \frac{H_{c0}}{\lambda_0}, \quad (\text{C4})$$

which is the depairing current density.

For $\Gamma = 0$, Eq. (C1) is a simple quadratic equation for ζ_d . Then the solution is given by

$$\zeta_{d0} = \frac{2}{\pi} + \frac{3\pi}{8} - \sqrt{\left(\frac{2}{\pi} + \frac{3\pi}{8}\right)^2 - 1} = 0.300. \quad (\text{C5})$$

$$\Delta_{d0} = \exp\left[-\frac{\pi}{4}\zeta_{d0}\right] = 0.790, \quad (\text{C6})$$

$$s_{d0} = \Delta_{d0}\zeta_{d0} = 0.237, \quad (\text{C7})$$

resulting in $j_d(0,0) = 0.595H_{c0}/\lambda_0$, the well-known result obtained by Maki [13, 14] and Kupriyanov and Lukichev [35].

For $0 \leq \Gamma \ll 1$, we can solve Eq. (C1) by expanding ζ_d about ζ_{d0} . Substituting

$$\zeta_d = \zeta_{d0} - \alpha \frac{\Gamma}{\Delta_{d0}}, \quad (\text{C8})$$

into Eq. (C1), we find

$$\alpha = \frac{1 + \pi/2 - 2(1 + 8/\pi)\zeta_{d0}}{2 + 3\pi^2/8 - \pi\zeta_{d0}} = 0.365, \quad (\text{C9})$$

Then Eqs. (C2) and (C3) result in

$$\Delta_d = e^{-\frac{\pi}{4}\zeta_d - \frac{\Gamma}{\Delta_d}} = \Delta_{d0} \exp\left[\left(\frac{\pi\alpha}{4} - 1\right)\frac{\Gamma}{\Delta_{d0}}\right], \quad (\text{C10})$$

$$s_d = \Delta_d \zeta_d = (s_{d0} - \alpha\Gamma) \exp\left[\left(\frac{\pi\alpha}{4} - 1\right)\frac{\Gamma}{\Delta_{d0}}\right] \quad (\text{C11})$$

Appendix D: Derivations of Eqs. (50) and (57)

1. Fast measurement

For $s \ll 1$ and $\Gamma \ll 1$, the superfluid density is given by Eq. (28). Then, Eq. (49) yields

$$\frac{L_k(s_{\text{bias}}, \Gamma, 0)}{L_{k0}} = 1 + \left(1 + \frac{2}{\pi}\right)\Gamma + \left(\frac{\pi}{4} + \frac{4}{3\pi}\right)s_{\text{bias}}, \quad (\text{D1})$$

then

$$\frac{L_k(s_{\text{bias}}, \Gamma, 0)}{L_k(0, \Gamma, 0)} = 1 + \left(\frac{\pi}{4} + \frac{4}{3\pi}\right)s_{\text{bias}}. \quad (\text{D2})$$

Here the current-momentum relation, Eq. (29), can be written as

$$\begin{aligned} s_{\text{bias}} &= \frac{1}{\pi} \left(\frac{j_{\text{bias}}}{j_{s0}}\right)^2 = \frac{1}{\pi} \left(\frac{j_d}{j_{s0}}\right)^2 \left(\frac{j_{\text{bias}}}{j_d}\right)^2 \\ &= s_d \left[\Delta_d(\Gamma) - \frac{4s_d(\Gamma)}{3\pi} - \frac{2\Gamma}{\pi}\right]^2 \left(\frac{j_{\text{bias}}}{j_d}\right)^2 \\ &\simeq s_{d0} \left(\Delta_{d0} - \frac{4s_{d0}}{3\pi}\right)^2 \left(\frac{j_{\text{bias}}}{j_d}\right)^2. \end{aligned} \quad (\text{D3})$$

Substituting Eq. (D3) into Eq. (D2), we find

$$\frac{L_k(s_{\text{bias}}, \Gamma, 0)}{L_k(0, \Gamma, 0)} = 1 + C_{\text{fm}} \left(\frac{j_{\text{bias}}}{j_d}\right)^2, \quad (\text{D4})$$

$$C_{\text{fm}} = \frac{3\pi^2 + 16}{12\pi} s_{d0} \left(\Delta_{d0} - \frac{4s_{d0}}{3\pi}\right)^2 = 0.136. \quad (\text{D5})$$

2. Slow measurement

Substituting the superfluid density, Eq. (28), for $s \ll 1$ and $\Gamma \ll 1$ into Eq. (55), we obtain

$$\frac{L_k(s_{\text{bias}}, \Gamma, 0)}{L_{k0}} = 1 + \left(1 + \frac{2}{\pi}\right)\Gamma + 3\left(\frac{\pi}{4} + \frac{4}{3\pi}\right)s \quad (\text{D6})$$

then

$$\frac{L_k(s_{\text{bias}}, \Gamma, 0)}{L_k(0, \Gamma, 0)} = 1 + 3\left(\frac{\pi}{4} + \frac{4}{3\pi}\right)s \quad (\text{D7})$$

Using Eq. (D3), we find

$$\frac{L_k(s, \Gamma, 0)}{L_k(0, \Gamma, 0)} = 1 + C_{\text{sm}} \left(\frac{j_s}{j_d}\right)^2, \quad (\text{D8})$$

$$C_{\text{sm}} = \frac{3\pi^2 + 16}{4\pi} s_{d0} \left(\Delta_{d0} - \frac{4s_{d0}}{3\pi}\right)^2 = 0.544. \quad (\text{D9})$$

Appendix E: Derivations of Eq. (64)

To evaluate Eq. (63) for small Γ regions, we rewrite Eqs. (24) and (25) in more convenient forms. Let us expand $\Delta(s, \Gamma, 0)$ around $\Delta(s, 0, 0)$ and write

$$\Delta(s, \Gamma, 0) = \Delta(s, 0, 0) - \beta\Gamma. \quad (\text{E1})$$

Substituting Eq. (E1) into Eq. (24), we find

$$\beta = \left(1 - \frac{\pi s}{4\Delta(s, 0, 0)}\right)^{-1}. \quad (\text{E2})$$

Then Eq. (25) yields

$$\frac{n_s(s, \Gamma, 0)}{n_{s0}} = \Delta(s, 0, 0) - \frac{\Gamma}{1 - \frac{\pi s}{4\Delta(s, 0, 0)}} - \frac{4s}{3\pi} - \frac{2\Gamma}{\pi} \quad (\text{E3})$$

Now Eq. (63) reduces to

$$\begin{aligned} \left(\frac{H_{sh}(\Gamma, 0)}{H_{c0}}\right)^2 &= \pi \int_0^{s_d} \left[\Delta(s, 0, 0) - \frac{\Gamma}{1 - \frac{\pi s}{4\Delta(s, 0, 0)}}\right] ds \\ &\quad - \frac{2}{3}s_d^2 - 2\Gamma s_d. \end{aligned} \quad (\text{E4})$$

Here s_d is given by Eq. (C11). To perform the integration, we change the variable from s to $z = s/\Delta(s, 0, 0)$. Using $d\Delta(s, 0, 0)/ds = -(\pi/4)[1 - \pi s/4\Delta(s, 0, 0)]^{-1}$ and $\Delta(s, 0, 0) = e^{-\pi z/4}$, we find $ds = dz/(dz/ds) = e^{-\pi z/4}(1 - \pi z/4)dz$. Then the integration becomes

$$\begin{aligned} &\int_0^{s_d} \left[\Delta(s, 0, 0) - \frac{\Gamma}{1 - \frac{\pi s}{4\Delta(s, 0, 0)}}\right] ds \\ &= \int_0^{z_d} \left[e^{-\frac{\pi z}{2}} \left(1 - \frac{\pi z}{4}\right) - \Gamma e^{-\frac{\pi z}{4}}\right] dz \\ &= \frac{1}{\pi} \left[1 - \left(1 - \frac{\pi z_d}{2}\right)e^{-\frac{\pi z_d}{2}} - 4\Gamma(1 - e^{-\frac{\pi z_d}{4}})\right] \end{aligned} \quad (\text{E5})$$

where $z_d = s_d/\Delta(s_d, 0, 0)$. To obtain z_d , we expand $\Delta(s_d, 0, 0)$ around $\Delta_d = \Delta(s_d, \Gamma, 0)$:

$$\Delta(s_d, 0, 0) = \Delta_d + \eta\Gamma. \quad (\text{E6})$$

Here Δ_d is given by Eq. (C10). Substituting Eq. (E6) into $\Delta(s_d, 0, 0) = \exp[-\pi s_d/\Delta(s_d, 0, 0)]$ and using $\Delta_d = \exp[-\pi s_d/\Delta_d - \Gamma/\Delta_d]$, we find

$$\eta = \left(1 - \frac{\pi\zeta_d}{4}\right)^{-1}, \quad (\text{E7})$$

where $\zeta_d = s_d/\Delta_d$ is given by Eq. (C8). Then we find

$$z_d = \frac{s_d}{\Delta_d + \eta\Gamma} = \zeta_d \frac{1 - \frac{\pi}{4}\zeta_d}{1 - \frac{\pi}{4}\zeta_d + \frac{\Gamma}{\Delta_d}}. \quad (\text{E8})$$

-
- [1] C. M. Natarajan, M. G. Tanner, and R. H. Hadfield, *Supercond. Sci. Technol.* **25**, 063001 (2012).
 - [2] A. Engel, J. J. Renema, K. Il'in, and A. Semenov, *Supercond. Sci. Technol.* **28**, 114003 (2015).
 - [3] J. Zmuidzinas, *Annu. Rev. Condens. Matter Phys.* **3**, 169 (2012).
 - [4] P. D. Mauskopf, *PASP* **130**, 082001 (2018).
 - [5] M. H. Devoret and R. J. Schoelkopf, *Science* **339**, 1169 (2013).
 - [6] G. Wendin, *Rep. Prog. Phys.* **80**, 106001 (2017).
 - [7] E. Grumbling and M. Horowitz, *Quantum computing: progress and prospects*. (The National Academy Press, Washington DC, 2019).
 - [8] H. Padamsee, *Supercond. Sci. Technol.* **30**, 053003 (2017).
 - [9] A. Gurevich, *Supercond. Sci. Technol.* **30**, 034004 (2017).
 - [10] D. B. Liarte, S. Posen, M. K. Transtrum, G. Catelani, M. Liepe, and J. P. Sethna, *Supercond. Sci. Technol.* **30**, 033002 (2017).
 - [11] T. Kubo, *Supercond. Sci. Technol.* **30**, 023001 (2017).
 - [12] K. Maki, Gapless superconductivity, in *Superconductivity*, edited by R. D. Parks (Marcel Dekker, Inc., New York, 1969), vol. 2, p. 1035.
 - [13] K. Maki, *Prog. Theor. Phys.* **29**, 10 (1963).
 - [14] K. Maki, *Prog. Theor. Phys.* **333**, 10 (1963).
 - [15] A. J. Kerman, E. A. Dauler, W. E. Keicher, J. K. W. Yang, K. K. Berggren, G. Gol'tsman, and B. Voronov, *Appl. Phys. Lett.* **88**, 111116 (2006).
 - [16] M. R. Vissers, J. Hubmayr, M. Sandberg, S. Chaudhuri, C. Bockstiegel, and J. Gao, *Appl. Phys. Lett.* **107**, 062601 (2015).
 - [17] N. Groll, A. Gurevich, and I. Chiorescu, *Phys. Rev. B* **81**, 020504(R) (2010).
 - [18] A. Romanenko, A. Grassellino, A. C. Crawford, D. A. Sergatskov, and O. Melnychuk, *Appl. Phys. Lett.* **105**, 234103 (2014).
 - [19] S. Huang, T. Kubo, and R. L. Geng, *Phys. Rev. Accel. Beams* **19**, 082001 (2016).
 - [20] S. Posen, M. Checchin, A. C. Crawford, A. Grassellino, M. Martinello, O. S. Melnychuk, A. Romanenko, D. A. Segatskov, and Y. Trenikhina, *J. Appl. Phys.* **119**, 213903 (2016).
 - [21] A. Romanenko and D. Schuster *Phys. Rev. Lett.* **119**, 264801 (2017).
 - [22] A. Romanenko, R. Pilipenko, S. Zorzetti, D. Frolov, M. Awida, S. Belomestnykh, S. Posen, and A. Grassellino, *Phys. Rev. Applied* **13**, 034032 (2020).
 - [23] S. Posen, A. Romanenko, A. Grassellino, O.S. Melnychuk, and D.A. Sergatskov, *Phys. Rev. Applied* **13**, 014024 (2020).
 - [24] R.L. Geng, G. V. Eremeev, H. Padamsee, and V. D. Shemelin, in *Proceedings of PAC07, Albuquerque, New Mexico, USA* (2007, JACoW), p. 2337.
 - [25] T. Kubo, Y. Ajima, H. Inoue, K. Umemori, Y. Watanabe, and M. Yamanaka, in *Proceedings of IPAC2014, Dresden, Germany* (2014, JACoW), p. 2519.
 - [26] A. Grassellino, A. Romanenko, Y. Trenikhina, M. Checchin, M. Martinello, O. S. Melnychuk, S. Chandrasekaran, D. A. Sergatskov, S. Posen, A. C. Crawford, S. Aderhold, and D. Bice, *Supercond. Sci. Technol.* **30**, 094004 (2017).
 - [27] P. Dhakal, S. Chetri, S. Balachandran, P. J. Lee, and G. Ciovati, *Phys. Rev. Accel. Beams* **21**, 032001 (2018).
 - [28] S. Posen, N. Valles, and M. Liepe, *Phys. Rev. Lett.* **115**, 047001 (2015).
 - [29] S. Keckert, T. Junginger, T. Buck, D. Hall, P. Kolb, O. Kugeler, R. Laxdal, M. Liepe, S. Posen, T. Prokscha, Z. Salman, A. Suter, and J. Knobloch, *Supercond. Sci. Technol.* **32**, 075004 (2019).
 - [30] A. Grassellino, A. Romanenko, D. Sergatskov, O. Melnychuk, Y. Trenikhina, A. Crawford, A. Rowe, M. Wong, T. Khabiboulline, and F. Barkov, *Supercond. Sci. Technol.* **26**, 102001 (2013).
 - [31] P. Dhakal, G. Ciovati, G. R. Myneni, K. E. Gray, N. Groll, P. Maheshwari, D. M. McRae, R. Pike, T. Proslir, F. Stevie, R. P. Walsh, Q. Yang, and J. Zasadzinski, *Phys. Rev. ST Accel. Beams* **16**, 042001 (2013).
 - [32] J. T. Maniscalco, D. Gonnella, and M. Liepe, *J. Appl. Phys.* **121**, 043910 (2017).
 - [33] Z. Yang, X. Lu, W. Tan, J. Zhao, D. Yang, Y. Yang, Y. He, and K. Zhou, *Appl. Surf. Sci.* **439**, 1119 (2018).
 - [34] D. Gonnella, S. Aderhold, A. Burrill, E. Daly, K. Davis, A. Grassellino, C. Grimm, T. Khabiboulline, F. Marhauser, O. Melnychuk, A. Palczewski, S. Posen, M. Ross, D. Sergatskov, A. Sukhanov, Y. Trenikhina, and K.M. Wilson, *Nucl. Instrum. Methods Phys. Res. A* **883**, 143 (2018).
 - [35] M. Yu Kupriyanov and V. F. Lukichev, *Sov. J. Low Temp. Phys.* **6**, 210 (1980).
 - [36] A. J. Annunziata, D. F. Santavicca, L. Frunzio, G. Catelani, M. J. Rooks, A. Frydman, and D. E. Prober, *Nanotechnology* **21**, 445202 (2010).
 - [37] J. R. Clem and V. G. Kogan, *Phys. Rev. B* **86**, 174521 (2012).
 - [38] V. P. Galaiko, *Sov. Phys. JETP* **23**, 475 (1966).
 - [39] G. Catelani and J. P. Sethna, *Phys. Rev. B* **78**, 224509 (2008).
 - [40] F. Pei-Jen Lin and A. Gurevich, *Phys. Rev. B* **85**, 054513 (2012).

- [41] V. Ngampruetikorn and J. A. Sauls, Phys. Rev. Research **1**, 012015 (2019).
- [42] J. Zasadzinski, Tunneling spectroscopy of conventional and unconventional superconductors, in *The Physics of Superconductors*, edited by K. H. Bennemann and J. B. Ketterson (Springer, Berlin, 2003), Vol. 1, p. 591.
- [43] C. Becker, S. Posen, N. Groll, R. Cook, C. M. Schlepütz, D. L. Hall, M. Liepe, M. Pellin, J. Zasadzinski, and T. Proslir, Appl. Phys. Lett. **106**, 082602 (2015).
- [44] N. R. Groll, G. Ciovati, A. Grassellino, A. Romanenko, J. F. Zasadzinski, and T. Proslir, arXiv:1805.06359 [cond-mat.supr-con].
- [45] R. C. Dynes, V. Narayanamurti, and J. P. Garno, Phys. Rev. Lett. **41**, 1509 (1978).
- [46] R. C. Dynes, J. P. Garno, G. B. Hertel, and T. P. Orlando, Phys. Rev. Lett. **53**, 2437 (1984).
- [47] F. Herman and R. Hlubina, Phys. Rev. B **94**, 144508 (2016).
- [48] F. Herman and R. Hlubina, Phys. Rev. B **96**, 014509 (2017).
- [49] F. Herman and R. Hlubina, Phys. Rev. B **97**, 014517 (2018).
- [50] A. Gurevich and T. Kubo, Phys. Rev. B **96**, 184515 (2017).
- [51] T. Kubo and A. Gurevich, Phys. Rev. B **100**, 064522 (2019).
- [52] T. Kubo, Phys. Rev. Research **2**, 013302 (2020).
- [53] A. Gurevich, Phys. Rev. Lett. **113**, 087001 (2014).
- [54] K. Maki, Prog. Theor. Phys. **31**, 731 (1964).
- [55] P. Fulde, Phys. Rev. **137**, A783 (1965).
- [56] A. Anthore, H. Pothier, and D. Esteve, Phys. Rev. Lett. **90**, 127001 (2003).
- [57] A. A. Abrikosov and L. P. Gorkov, Soviet Phys. JETP **12**, 1243 (1961).
- [58] P. Fulde and K. Maki, Phys. Rev. **141**, 275 (1966).
- [59] W. Belzig, C. Bruder, and G. Schon, Phys. Rev. B **54**, 9443 (1996).
- [60] W. Belzig, F. K. Wilhelm, C. Bruder, G. Schon, and A. D. Zaikin, Superlattices Microstruct. **25**, 1251 (1999).
- [61] G. Eilenberger, Z. Phys. **214**, 195 (1968).
- [62] A. I. Larkin and Yu. N. Ovchinnikov, Sov. Phys. JETP **28**, 1200 (1969).
- [63] K. D. Usadel, Phys. Rev. Lett. **25**, 507 (1970).
- [64] N. B. Kopnin, *Theory of Nonequilibrium Superconductivity*. (Oxford University Press, 2001).
- [65] J. Romijn, T. M. Klapwijk, M. J. Renne, and J. E. Mooij, Phys. Rev. B **26**, 3648 (1982).
- [66] A. Yu Rusanov, M. B. S. Hesselberth, and J. Aarts, Phys. Rev. B **70**, 024510 (2004).
- [67] Y. Sun, H. Ohnuma, S. Ayukawa, T. Noji, Y. Koike, T. Tamegai, and H. Kitano, arXiv:1911.00727 [cond-mat.supr-con].
- [68] S. M. Anlage, H. J. Snortland, and M. R. Beasley, IEEE Trans. Magn. **25**, 1388 (1989).
- [69] D. F. Santavicca, J. K. Adams, L. E. Grant, A. N. McCaughan, and K. K. Berggren, J. Appl. Phys. **119**, 234302 (2016).
- [70] D. Xu, S. K. Yip, and J. A. Sauls, Phys. Rev. B **51**, 16233 (1995).
- [71] A. Gurevich, Appl. Phys. Lett. **88**, 012511 (2006).
- [72] T. Kubo, Y. Iwashita, and T. Saeki, Appl. Phys. Lett. **104**, 032603 (2014).
- [73] A. Gurevich, AIP Adv. **5**, 017112 (2015).
- [74] L. Kramer, Phys. Rev. **170**, 475 (1968).
- [75] M. K. Transtrum, G. Catelani, and J. P. Sethna, Phys. Rev. B **83**, 094505 (2011).
- [76] W. Zhang, Q. Jia, L. You, X. Ou, H. Huang, L. Zhang, H. Li, Z. Wang, and X. Xie, Phys. Rev. Applied **12**, 044040 (2019).
- [77] D. Niepce, J. Burnett, and J. Bylander, Phys. Rev. Applied **11**, 044014 (2019).
- [78] Y. Iwashita, Y. Tajima, and H. Hayano, Phys. Rev. ST Accel. Beams **11**, 093501 (2008).
- [79] M. Ge, G. Wu, D. Burk, J. Ozelis, E. Harms, D. Sergatskov, D. Hicks, and L. D. Cooley, Supercond. Sci. Technol. **24**, 035002 (2011).
- [80] Y. Yamamoto, H. Hayano, E. Kako, S. Noguchi, T. Shishido, and K. Watanabe, Nucl. Instrum. Methods Phys. Res. A **729**, 589 (2013).
- [81] M. Wenskat, JINST **14** P06021 (2019).
- [82] U. Pudasaini, G. Ereameev, C. E. Reece, J. Tuggle, and M. J. Kelley, Supercond. Sci. Technol. **33**, 045012, (2020).
- [83] J. Knobloch, R. L. Geng, M. Liepe, and H. Padamsee, in *proceedings of SRF 1999, La Fonda Hotel, Santa Fe, New Mexico, USA* (1999, JACoW), p.77.
- [84] T. Kubo, Prog. Theor. Exp. Phys. **2015**, 063G01 (2015).
- [85] T. Kubo, Prog. Theor. Exp. Phys. **2015**, 073G01 (2015).
- [86] C. Xu, C. E. Reece, and M. J. Kelley, Phys. Rev. Accel. and Beams **19**, 033501 (2016).
- [87] C. Z. Antoine, J. C. Villegier, and G. Martinet, Appl. Phys. Lett. **102**, 102603 (2013).
- [88] T. Tan, M. A. Wolak, X. X. Xi, T. Tajima, and L. Civala Sci. Rep. **6**, 35879 (2016).
- [89] A-M. Valente-Feliciano, Supercond. Sci. Technol. **29**, 113002 (2016).
- [90] C. Z. Antoine, M. Aburas, A. Four, F. Weiss, Y. Iwashita, H. Hayano, S. Kato, T. Kubo, and T. Saeki, Supercond. Sci. Technol. **32**, 085005 (2019).
- [91] T. Kubo, Jpn. J. Appl. Phys **58**, 088001 (2019).
- [92] H. Ito, H. Hayano, T. Kubo, and T. Saeki, Nucl. Instrum. Methods Phys. Res. A **955**, 163284 (2020).
- [93] R. Ito, T. Nagata, H. Hayano, R. Katayama, T. Kubo, T. Saeki, Y. Iwashita, and H. Ito, in *proceedings of SRF2019, Dresden, Germany* (2019, JACoW), p. 630.
- [94] H. Ito, H. Hayano, T. Kubo, T. Saeki, R. Katayama, Y. Iwashita, H. Tongu, R. Ito, T. Nagata, and C. Z. Antoine, in *proceedings of SRF2019, Dresden, Germany* (2019, JACoW), p. 634.
- [95] S. Keckert, J. Knobloch, O. Kugeler, D. Tikhonov, and A-M. Valente-Feliciano, in *proceedings of SRF2019, Dresden, Germany* (2019, JACoW), p. 802.
- [96] R. Katayama, H. Hayano, T. Kubo, T. Saeki, H. Ito, Y. Iwashita, H. Tongu, C.Z. Antoine, R. Ito, and T. Nagata, in *proceedings of SRF2019, Dresden, Germany* (2019, JACoW), p. 809.
- [97] T. Oseroff, M. Liepe, Z. Sun, B. Moeckly, and M. Sowa, in *proceedings of SRF2019, Dresden, Germany* (2019, JACoW), p. 952.
- [98] E. Thoeng, T. Junginger, P. Kolb, B. Matheson, G. Morris, N. Muller, S. Saminathan, R. Baartman, and R. E. Laxdal, in *proceedings of SRF2019, Dresden, Germany* (2019, JACoW), p. 966.
- [99] D. Turner, O. B. Malyshev, G. Burt, T. Junginger, L. Gurran, K. D. Dumbell, A. J. May, N. Pattalwar, and S. M. Pattalwar in *proceedings of SRF2019, Dresden,*

Germany (2019, JACoW), p. 970.

[100] I. H. Senevirathne, G. Ciovati, and J. R. Delayen, in *proceedings of SRF2019, Dresden, Germany* (2019, JACoW), p. 980.